11 Satellite Altimetry in Coastal Regions

Paolo Cipollini, Jérôme Benveniste, Florence Birol, M. Joana Fernandes, Estelle Obligis, Marcello Passaro, P. Ted Strub, Guillaume Valladeau, Stefano Vignudelli, and John Wilkin

GLOSSARY

1DVAR:	One-Dimensional VARiational scheme
ACCRA:	Atmospheric Correction for Coastal Radar Altimeters
ALADIN:	Aire Limitée Adaptation dynamique Développement InterNational (model)
ALBICOCCA:	ALtimeter-Based Investigations in COrsica, Capraia and Contiguous Area
ALES:	Adaptive Leading-Edge Subwaveform retracker
ARCOM:	Altimetry for Regional and Coastal Ocean Modeling
AVISO:	Archiving, Validation and Interpretation of Satellite Oceanographic Data
CAW:	Coastal Altimetry Workshop
CCI:	Climate Change Initiative
CNES:	Centre National d'Études Spatiales
COASTALT:	ESA COASTal ALTtimetry - Development of radar altimetry data processing in the oceanic coastal zone
COSS-TT:	Coastal Ocean and Shelf Seas Task Team of GODAE,
COSTA:	COastal Sea level Tailored ALES
CSIRO:	Commonwealth Scientific and Industrial Research Organisation
CTOH:	Center for Topographic studies of the Ocean and Hydrosphere
DAC:	Dynamic Atmosphere Correction
DLM:	Dynamically Linked Model
DLR:	Deutsches Zentrum für Luft- und Raumfahrt (German Aerospace Center)
DMSP:	Defense Meteorological Satellite Program
DTC:	Dry Tropospheric Correction
ECMWF:	European Center for Medium-range Weather Forecasts
EnOI:	Ensemble Optimal Interpolation
ERA:	ECMWF ReAnalysis
ERS-1:	European Remote Sensing satellite-1
ERS-2:	European Remote Sensing satellite-2
ESA:	European Space Agency
FASTEM:	FAST microwave Emissivity Model
FOV:	Field of View
GDR:	Geophysical Data Records
GFO:	GEOSAT Follow-On
GLORYS:	Global Ocean ReanalYsis and Simulation
GNSS:	Global Navigation Satellite System
GODAE:	Global Ocean Data Assimilation Experiment
GPD:	GNSS derived Path Delay
G-POD:	ESA Grid Processing On Demand

GPS: Global Positioning System
GPT: Global Pressure and Temperature
IB: Inverse Barometer
JPL: Jet Propulsion Laboratory
LCA: Land Contamination Algorithm
LEGOS: Laboratoire d'Études en Géophysique et Océanographie Spatiales
LRM: Low-Resolution Mode
MDT: Mean Dynamic Topography
MHS: Microwave Humidity Sounder
MLE3: Maximum-Likelihood Estimation of 3 parameters
MOG2D: Modèle aux Ondes de Gravité - 2 dimensions
MPA: Mixed-Pixel Algorithm
MWR: Microwave Radiometers
NASA: National Aeronautics and Space Administration
NCEP: National Centers for Environmental Prediction
NOAA: National Oceanic and Atmospheric Administration
NPC: NOAA Prediction Center
NWM: Numerical Weather Models
NWS: National Weather Service
ODES: Online Data Extraction Service
PEACHI: Prototype for Expertise on AltiKa for Coastal, Hydrology and Ice
PISTACH: Prototype Innovant de Système de Traitement pour les Applications Côtières et l'Hydrologie
PLRM: Pseudo-Low Resolution Mode
POD: Precise Orbit Determination
PO.DAAC: Physical Oceanography Distributed Active Archive Center
RADS: Radar Altimetry Database System
RMS: Root Mean Square
SAR: Synthetic Aperture Radar
SARAL: Satellite with ARgos and ALtiKa
SGDR: Sensor Geophysical Data Record
SLA: Sea Level Anomaly
SLP: Sea Level Pressure
SSB: Sea State Bias
SSHA: Sea Surface Height Anomaly
SSM/I: Special Sensor Microwave Imager
SST: Sea Surface Temperature
SWH: Significant Wave Height
SWOT: Surface Water Ocean Topography
T-UGO: Toulouse Unstructured Grid Ocean model
TB: Brightness Temperature
TG: Tide Gauge
T/P: TOPEX/Poseidon
WTC: Wet Tropospheric Correction

11.1 INTRODUCTION AND RATIONALE

The ocean plays a major role in the climate system and its evolution, not only as a regulator but also as an indicator of changes. These changes are mostly felt in the coastal zone, where they affect local populations, biodiversity, accessible marine resources, and coastal engineering and management. The coastal zone is where changing circulation, sea level, and sea state have by far the largest impact

on human society. Knowledge of ocean dynamics is essential, but near the coast the processes are much more complex than in the open ocean and require dedicated observing tools. Coastal observations are also required for marine meteorology forecasting and climate predicting models.

The success of altimetry over the open ocean, which is illustrated in detail in the previous and following chapters of this book, leads most naturally to consider the potential of this remote sensing technique in the coastal zone, the natural interface between the oceans and humans.

In the last 15 years, increasing international efforts have been put toward the improvement and exploitation of altimetry in the coastal zone, a broad field of research, development, and applications that is now routinely called *coastal altimetry* and was first reviewed in a book with the same name in 2011 (Vignudelli et al. 2011). In this chapter, we describe both the improvements in coastal altimetry on the technical side and the ensuing applications.

The technical improvements derive from the combination of three approaches that have been developed in coastal altimetry. They are, in the chronological order in which they have appeared: (1) more detailed and coastal-specific data editing; (2) improvements in key correction fields; and (3) new schemes for radar echo analysis (retracking) optimizing the retrieval of the leading edge of the radar return signal (waveform). In more detail:

1. Historically, some research initiatives made progress by abandoning the systematic rejection of along-track data considered as suspect because of the water depth or their proximity to land. For example, in the ALBICOCCA project (Altimeter-Based Investigations in Corsica, Capraia, and Contiguous Area, and funded by Centre National d'Études Spatiales [CNES]), the data in shallower water and closer to land were examined and evaluated based on separate editing criteria for individual correction terms, range, and finally deriving the sea level anomalies (SLAs); the X-TRACK post-processing algorithm is derived from this approach and now routinely produces regional altimetry products that are largely distributed (Birol et al. 2016). Similarly, Feng and Vandemark (2011) showed that a significant volume of data could be reclaimed in the coastal zone by judicious application of standard data quality flags, especially the rain flag, and a revised wet troposphere range correction.
2. At the same time, improvements in the geophysical and propagation corrections that have to be applied to the altimeter range (see previous chapters, as well as the Radar Altimetry Tutorial at www.altimetry.info for a description of the altimetry measurement and its corrections) have significantly increased the accuracy of the basic retrieved data that were subjected to the detailed editing. The range correction that has had the most significant upgrade in the coastal zone is the wet tropospheric correction, which we discuss in Section 11.3.2; tidal models and dynamic atmospheric corrections have also had significant advances as we illustrate in 11.3.3.
3. Finally, retracking methods have been designed to accommodate nonstandard waveforms caused by proximity to land, such as the algorithm developed in the PEACHI project for Ka-band radars (Valladeau et al. 2015; see Section 11.4.1). Another specific approach is to restrict the tracking to the leading edge portion of the radar return, as carried out by the ALES algorithm (Passaro et al. 2014; see Section 11.4.2). This allows the range measurement to be retrieved using only the footprint radius of the radar reflection (i.e., neglecting the information in the tail of the waveform which in the coastal zone is usually the first to be corrupted by artifacts as we will illustrate in Section 11.4.2).

The other innovation in altimeter data analysis important for coastal studies is the retrieval of the height signal from wide rivers (and their estuaries) and flood plains. These developments, which are discussed in Chapter 14 of this book, allow an estimate of river discharges into the coastal ocean in some cases, especially for large rivers and during high discharges, when the river inputs have their greatest effects.

Coastal applications of altimeter data are now becoming widespread and are presented and discussed in Sections 11.5 and 11.6. We expect some applications to take advantage of a unique prerogative of coastal altimetry (i.e., that, being global, it provides measurements over remote stretches of the world's coasts where there are no other observing devices). In many cases, those measurements go back to 1991–1992 (i.e., the start of the European Remote Sensing [ERS]-1 and TOPEX/Poseidon [T/P] missions). In all coastal applications, two basic limitations of altimeter sampling remain: the wide spatial separation of the altimeter tracks and the long periods (usually 10 days or more) between repeat passes over the same track (or within a few kilometers for non-exact-repeat orbits). These limitations are important in the coastal domain, where temporal and spatial scales of physical processes decrease as land is approached and depths also decrease. The availability of data from multiple altimeters reduces the impact of these problems somewhat, but the fact remains that coastal altimetry will normally yield stronger benefits if it is integrated with *in situ* observations and models that it can complement synergistically.

Assimilation of altimeter data into coastal ocean circulation models may make the best use of the altimeter data in addressing shorter time and space scales. Altimeter data that are not assimilated are also useful in providing validation of the circulation models. In these ways, altimeter data constitute a unique component and powerful constraint within the hybrid monitoring systems needed to understand and predict the complex and rapidly changing coastal ocean environment.

In this chapter, we first examine the improvements in altimeter processing in the coastal zone following the order in which they appear in the altimeter processing chain, i.e., first improvements in retracking in Section 11.2, then improvements in corrections in Section 11.3, and then in Section 11.4 we describe the diverse data set now available for coastal altimetry. These are enabling applications: those that rely on observations alone are described in Section 11.5, while those that exploit the synergy with models are in Section 11.6.

11.2 DEALING WITH COASTAL WAVEFORMS

11.2.1 Pulse-Limited Waveforms

The Brown waveform model (Brown 1977) described in Chapter 1 of this book remains to date the fundamental model for the estimation of geophysical parameters from pulse-limited altimetry. As confirmed by the PISTACH project (Prototype Innovant de Système de Traitement pour les Applications Côtières et l'Hydrologie) (Mercier et al. 2010), in which a classification of Jason-1 waveforms was carried out, the Brown model is a good approximation for more than 90% of the waveforms over the open ocean, up to about 10–15 km from the coast. This is clearly seen in Figure 11.1 taken from Halimi et al. (2013), which shows the percentage of waveforms in three different classes as a function of distance from coast. Two questions then arise. The first question, which is central to coastal altimetry, is how we deal with the non-Brownian waveforms in the last 10–15 km. As one can see in the figure, these become more and more frequent (more than 50% at 5 km from the coastline) as one approaches the coast. The second question is whether that 7%–8% of non-Brownian waveforms away from the coast contain information that is not retrieved by standard processing, and if yes, how we can recover that information. (There is a hint that techniques that we develop for the coastal zone also may find applicability over the open ocean for those nonstandard waveforms, as will be discussed later in the chapter.)

Departures of pulse-limited power waveforms from the Brown model are caused by variations of the surface height statistics and backscatter within the radar footprint. These non-homogeneities may occur over the open ocean due to intense fronts, sub-mesoscale activity, and natural or man-made slicks. In the coastal zone, they are also caused by the effects of shallow bathymetry, the sheltering of the sea induced by the coastal morphology, and the contamination by land entering the footprint. One particular case is the radar echo contamination caused by the very strong signal reflected from calm water in a marina or coastal recess, such as a sheltered bay.

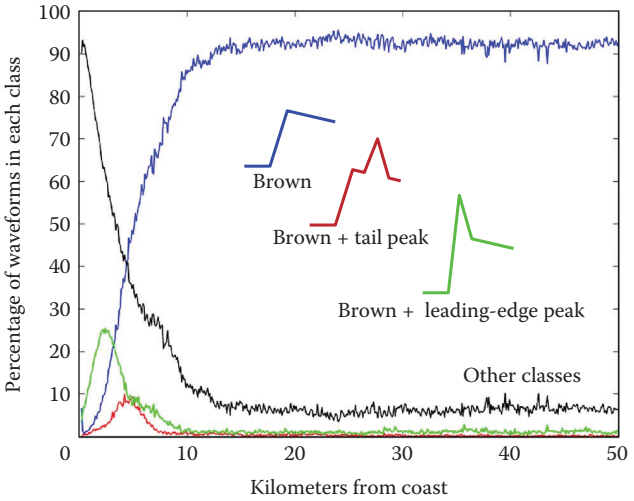

FIGURE 11.1 Percentages of observed classes of altimetric waveforms, as a function of distance from the coast, as found by the PISTACH project. (Reprinted from Halimi, A., et al., *IEEE Trans. Geosci. Rem. Sens.*, 1568–1577, 2013. With permission. © 2013 IEEE.)

Gómez-Enri et al. (2010) have studied the issue of contamination due to calm water with an example from overpasses of Envisat over a Mediterranean island; they confirmed that the signature of bright targets migrates following a hyperbolic law in the stack of sequential waveforms, which is expected on the basis of simple geometric considerations. As the altimeter extended footprint (i.e., the portion of the surface illuminated by the full waveform not just the leading edge) passes over the bright feature, the resulting peak in power moves from the tail of the waveform toward the leading edge and back, as is clearly visible in the example in Figure 11.2. Whether the peak reaches the leading edge or not depends on whether it is enough close to nadir and on its elevation. Targets at a height of several meters above sea level, such as the decks of large ships or flat icebergs, may generate signatures in the portion of the waveform preceding the leading edge (the "thermal noise" section); this concept is at the basis of studies identifying ships or icebergs in altimeter data (Tournadre et al. 2006, 2008). Similar considerations apply to dim features (i.e., areas of reduced backscatter such as those that may be caused by a low-lying island or sandbank). In this case, the waveform will show a power dip.

A comprehensive overview of retracking methods is in Gommenginger et al. (2011). Passaro et al. (2014) have reviewed the different approaches taken in literature for the processing of coastal pulse-limited waveforms that do not conform to the Brown model. There are four main approaches:

1. Algorithms based on some form of classification of the waveforms depending on their shape and the use of a different functional form for the fitting of each class. This approach, pioneered by Deng and Featherstone (2006), has then been used by Andersen (2010), Berry et al. (2010), and Yang et al. (2012).
2. Empirical models of the waveforms—for instance, using threshold values for the retracking in the presence of more peaky waveforms (Deng and Featherstone 2006; Hwang et al. 2006; Bao et al. 2009; Lee et al. 2010).
3. The processing of a stack of successive waveforms to detect the signature of bright targets as presented by Gómez-Enri et al. (2010) for the purpose of "cleaning" the stack prior to retracking (Quartly 2010).
4. The fitting of a portion of the waveform ("sub-waveform") containing the leading edge but excluding the tail section where most artifacts appear due to bright targets. This approach

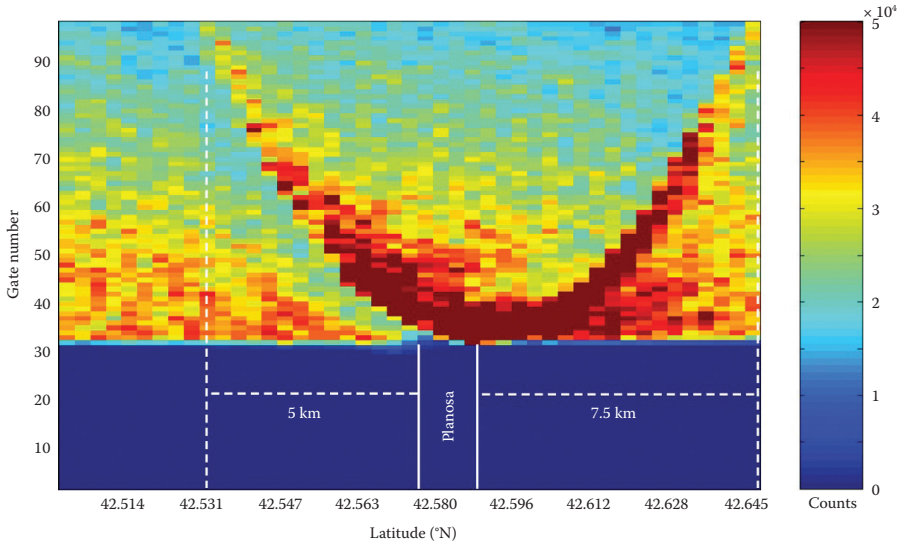

FIGURE 11.2 Envisat RA-2 power waveforms for orbital cycle 49, track 128 overpassing Pianosa Island in the Mediterranean Sea. Each column in the plot is a 20-Hz waveform (i.e., along the vertical axis are the receiving window power bins, also called gates). The horizontal axis represents the flight path of the satellite plotted by latitude; the color scale is in unit of power counts, corrected for automatic gain control variations. The vertical white lines mark the limits of the island. The bright hyperbolic feature is most likely due to a strong radar return from a sheltered bay on the northern side of the island. (Reprinted from Gómez-Enri, J., et al., *IEEE Geosci. Rem. Sens. Lett.*, 7, 474–478, 2010. With permission. © 2010 IEEE.)

was first presented in the PISTACH project for the so-called "RED" (for *reduced* portion of waveform) retracker (Mercier et al. 2009, 2010) and has since been adopted and developed by several authors (Guo et al. 2010; Yang et al. 2011; Idris and Deng 2012; Yang et al. 2012; Passaro et al. 2014).

The sub-waveform approach is emerging as the most promising one. This can be explained with the following intuitive considerations on the fitting process. As explained in detail in Chapter 1 of this book, properties of the leading edge yield the three main altimeter observables: range (derived from the leading edge position), significant wave height (from the leading edge rise time), and wind (from the maximum amplitude reached by the leading edge). A maximum likelihood estimator solving for these three parameters (MLE3) should in principle be able to give a good estimate of those parameters by fitting the leading edge portion only of the waveform, provided an independent estimate of a further variable in Brown's model, the off-nadir pointing angle or mispointing, is available from the onboard star trackers.* The tail of the waveform would normally not add information on the three main parameters and can be used instead to estimate mispointing in a four-parameter retracking scheme. In practice, for waveforms that conform well to the Brown model, such as those gathered in homogeneous open-ocean conditions where the noise is exclusively Raleigh, that is, speckle (plus a relatively small thermal noise), the use of the whole waveform in an MLE3 scheme helps constrain the fitting and improve the precision; reducing the fitting window under these "optimal" circumstances yields suboptimal estimates, as clearly illustrated by Passaro et al. (2014) with a Monte Carlo simulation. Conversely, in all those cases where the tail of the waveform is affected by artifacts due to non-homogeneities in the extended footprint (such as when bright targets

* Star trackers on board altimetric missions provide the precise pointing knowledge required for radar altimeter by pointing a great number of stars.

are present), fitting the whole waveform also has to accommodate the corrupted tail and therefore compromises the precision in the retrieval of the leading edge properties. In those latter cases, an approach that somehow reduces the fitting window to encompass only the leading edge option, or the leading edge plus a relatively small portion of the tail, may well be more robust. It must be noted that when the leading edge of the waveform is corrupted (which for instance may happen due to an off-nadir bright target at an elevation above the sea surface), then the sub-waveform approach is prone to significant errors.

In an Adaptive Leading-Edge Subwaveform (ALES) retracker, the retracking of each waveform is performed in two passes. A first pass looks at the rising portion of the waveform and provides a rough estimate of the significant wave height (SWH) from the slope of that portion. This estimate is then entered into an algorithm that selects the sub-waveform (i.e., sets the width of the fitting window over which a Brown fitting is performed in the second pass). Figure 11.3, taken from Passaro et al. (2014), shows three examples of Jason-2 waveforms in various conditions and the corresponding sub-waveform fit by the ALES retracker. As it can be seen, the width of the fitting window varies with the SWH; it can also be observed, in the middle panel referring to a coastal case, that the sub-waveform approach is not affected by a disturbance (likely from a bright target) in the tail portion of the waveform and therefore still achieves a good fit of the leading edge.

11.2.2 SAR Waveforms

SAR altimetry is intrinsically promising for coastal applications by virtue of the higher signal-to-noise ratio and along-track resolution; in SAR mode, a pulse repetition frequency higher than conventional altimetry allows slicing of the footprint in bands perpendicular to the flight direction by exploiting the Doppler frequency shift of the radar echoes from targets fore and aft of the satellite nadir point, resulting in a much higher along-track spatial resolution (300 m). However, this is only an advantage when the satellite crosses the coast at an angle that is close to normal to the coastline. When the ground track is more oblique to the coast, the SAR footprint (which extends in the across-track dimension and is essentially pulse-limited in that dimension) will encounter land and adversely impact the radar echo. Some experimental techniques have been proposed to account for all those non-optimal cases in which land or bright targets enter the footprint. Egido (2014) has used a coastal digital elevation model (DEM) and accurate geolocation of the echoes to reject those portions of the echoes that come from land. A sub-waveform approach has also been proposed for SAR waveforms by Thibaut et al. (2014). This is an area where research has only recently started, but more studies are expected to arise due to the availability of global SAR mode data from Sentinel-3 and the need to exploit in full the potential of this mission over the coastal zone.

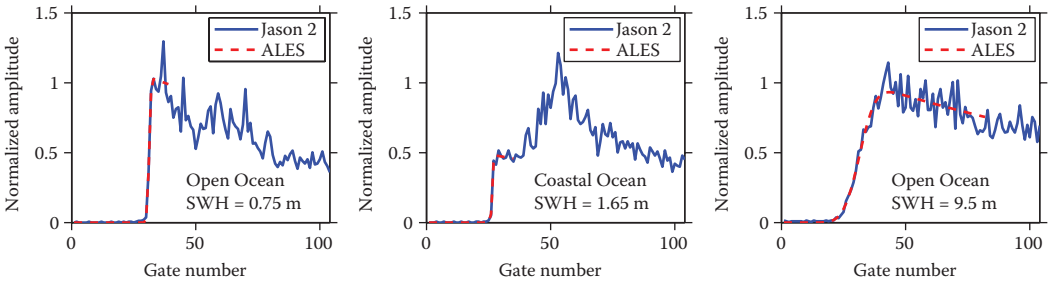

FIGURE 11.3 Examples of ALES retracking of Jason-2 waveforms in various conditions. (From Passaro, M., et al., *Rem. Sens. Environ.*, 145, 173–189, 2014.) Available under the terms of the Creative Commons BY 3.0 License.

11.3 IMPROVEMENTS IN RANGE AND GEOPHYSICAL CORRECTIONS

The accurate retrieval of sea surface height from satellite altimetry with centimeter-level accuracy requires the knowledge of all terms involved in the altimeter measurement system with similar or better accuracy, namely: satellite height above a reference ellipsoid from precise orbit determination (POD); altimeter range from dedicated retracking, including all instrument effects; and all range and geophysical corrections. As detailed in Chapter 1 of this book, a full set of range and geophysical corrections must be modeled and applied to altimetry: dry troposphere, wet troposphere, ionosphere, sea state bias, dynamic atmospheric correction, solid earth tide, ocean tide, load tide, and pole tide. The first four terms are the range corrections required to account for the interaction of the radar signal with the atmosphere and with the sea surface; the others refer to geophysical phenomena that need to be removed in order to separate them from the signal of interest, unless those phenomena are part of the very process that we aim to observe (as is, for instance, the case of the dynamic atmospheric contribution to storm surges).

The corrections with particular issues in the coastal regions are mainly the wet tropospheric correction (WTC), the sea state bias (SSB), and to somewhat lesser extent the dry tropospheric correction (DTC). Ocean tides may or may not be removed depending on the application; for example, models that simulate tides would retain this signal during data assimilation. Research is ongoing on these corrections and the main findings are detailed in the following subsection; the sole exception for this is the SSB, for which at the time of this writing we are not aware of any specific study to derive a solution for the coastal ocean—neither for conventional (pulse-limited) altimetry nor for SAR altimetry.

11.3.1 Dry Troposphere

The dry tropospheric correction (DTC) accounts for the path delay due to the dry neutral gases in the atmosphere. With an absolute value of about 2.3 m at sea level and a range of 0.2 m, the DTC is the largest range correction in satellite altimetry. However, using surface pressure from *in situ* observations or from an atmospheric model, such as those from the European Center for Medium-range Weather Forecasts (ECMWF), the DTC can be retrieved globally with an accuracy better than 1 cm, using the modified Saastamoinen model (Davis et al. 1985):

$$\Delta R_{dry} = - \frac{0.0022768\ p_s}{1 - 0.00266 cos\,(2\varphi) - 0.28 \cdot 10^{-6}\ h_s} \tag{11.1}$$

where p_s is the surface pressure in hPa, φ is the geodetic latitude, h_s is the surface height above the geoid (in meters), and the DTC, ΔR_{dry}, results in meters.

The DTC has an almost linear dependence on height of about 2.5 cm per each 100 m, directly related with the dependence of atmospheric pressure on height, which, according to Hopfield (1969) can be modeled as:

$$p_s = p_0\ exp\left[-\frac{g_m (h_s - h_0)}{R T_m} \right] \tag{11.2}$$

In Equation (2), p_0 is the sea level pressure (SLP) at height $h_0 = 0$, p_s is the surface pressure at height h_s, R is the specific constant for dry air, T_m is the mean temperature (in K) of the layer between heights h_0 and h_s, and g_m is the mean gravity; T_m can be estimated as the mean value of temperatures T_0 and T_s at heights h_0 and h_s, respectively, obtained, for example, from the values of T_0 at mean sea level given by the Global Pressure and Temperature (GPT) model (Boehm et al. 2007) and considering a value of $-0.0065\ Km^{-1}$ for the normal lapse rate of temperature with height.

The best sources of atmospheric pressure are the ECMWF Operational model (Miller et al. 2010) or the ECMWF ReAnalysis (ERA)-Interim model (Dee et al. 2011), provided as global grids at 0.125° × 0.125° (or better) and 0.75° × 0.75° spatial sampling, respectively, and 6-h intervals. The first model is not uniform, having undergone several updates. For this reason, for delayed-time products such as the geophysical data records (GDRs), ERA-Interim is the best model for the whole altimeter era, while ECMWF Operational is the most accurate model after 2004 (Fernandes et al. 2014; Legeais et al. 2014).

The DTC is provided in altimeter products as along-track interpolated values derived either from SLP or from surface pressure. In the first case, the derived DTCs are appropriate for use in coastal areas, having the same accuracy as in the open ocean. In the last case, in steep coastal areas, surrounded by land with elevations of, for example, 500–1000 m, errors in the DTC up to 5 cm or more (as shown in the example in Figure 11.4), increasing linearly as the coast is approached, may occur (Fernandes et al. 2014). These errors are systematic and will affect the derivation (e.g., of surface currents) in these regions. For a review of DTC errors in the context of inland water studies, in some aspects similar to those in the coastal regions, see for instance Fernandes et al. 2014.

11.3.2 Wet Troposphere

With an absolute value of less than 50 cm but with large space–time variability, the WTC is one of the major error sources, particularly in coastal altimetry.

In spite of the continuous progress in the modeling of the WTC by means of numerical weather models (NWMs) (e.g., Miller et al. 2010), an accurate enough retrieval of this effect can only be achieved through actual observations of the atmospheric water vapor content at the time and location of the altimetric measurements. For this purpose, dedicated microwave radiometers (MWRs) have been embedded in most altimetric missions.

Two main types of nadir-looking radiometers have been deployed in the altimetric satellites: two-band in ERS-1, ERS-2, Envisat, GEOSAT Follow-On (GFO), SARAL, and Sentinel-3, and three-band on T/P, Jason-1, Jason-2, and Jason-3. All of them have one band in the water vapor absorption line between 21 and 23.8 GHz plus one or two in "atmospheric window" channels, required to account for the effect of surface emissivity and for the cloud scattering (surface roughness is accounted for through the altimeter backscattering coefficient in a two-band configuration).

The algorithms used to retrieve the WTC from the measured brightness temperatures of the various MWR channels assume a surface ocean emissivity and are valid for ocean conditions, light rain, and

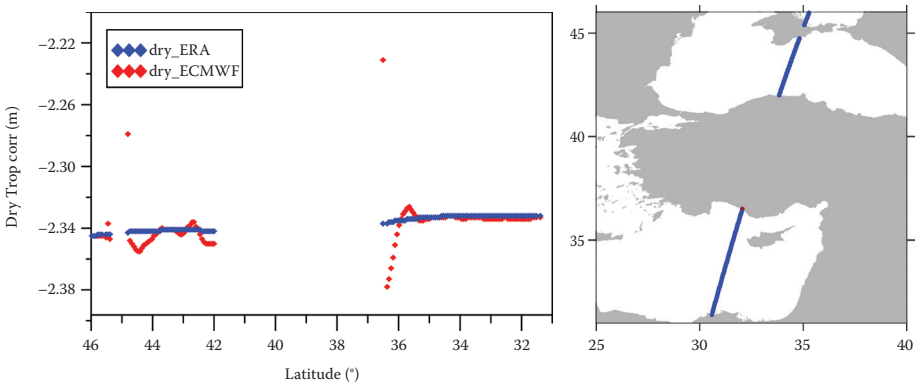

FIGURE 11.4 Illustration of DTC errors along Envisat cycle 12, pass 128 over the Mediterranean Sea and the Black Sea. The DTC from ERA-Interim is provided at sea level, while ECMWF Operational is provided at the height of model orography.

wind speed lower than 20 ms^{-1} (Obligis et al. 2006; Picard et al. 2015). Therefore, in the presence of surfaces with different emissivity, such as land or ice, the measurements lie outside the range of validity of the retrieval algorithm (Desportes et al. 2007). Thus, in spite of the high accuracy of MWR-derived WTC in open ocean, hampered by the contamination from land, ice, and rain in the radiometer footprint, the correction may be highly degraded, particularly in coastal and polar regions. Consequently, most current altimeter products fail to provide valid MWR-derived WTC in these regions.

It is worth noting that, with the contamination being directly related to the largest –3 dB width of the antenna pattern among the different channels, an instrument with a sharp spatial resolution, such as AltiKa (8 and 12 km at 23.8 and 37 GHz, respectively) (Valladeau et al. 2015), presents a very low contamination level, mainly occurring in the last 10 km approaching the coast (thin solid line in Figure 11.5). This raises the interest on higher frequency measurements (e.g., 89 GHz) offering a smaller footprint (see the following dedicated section).

In addition to contamination issues, noisy values caused by instrumental problems, jumps, and drifts may also occur in one or more channels, as illustrated by Scharroo et al. (2004).

In recent years, six main approaches have been proposed for correcting the altimeter measurements in the coastal regions, where the estimation from MWR measurements become invalid: (1) Basic extrapolation of the last valid measurement over the ocean; (2) a dynamically linked model (DLM) or composite approach; (3) the Land Contamination Algorithm (LCA); (4) the Mixed-Pixel Algorithm (MPA); (5) the GNSS (Global Navigation Satellite System) derived Path Delay (GPD) approach; and (6) variational method.

The first method is actually basic: The last valid brightness temperature (BT) measurement over ocean is extrapolated up to the coast. Validity in this context stands for non-contamination by land and is defined by a threshold on the land proportion in the field of view (FOV), estimated from a high-resolution land-sea mask and the theoretical half width of the FOV. This algorithm is applied on Envisat, Sentinel-3, and AltiKa (bold solid line on Figure 11.5) MWR.

The second method (DLM) was first used by Fernandes et al. (2003) and has been implemented in the European Space Agency's (ESA) COASTALT (COASTal ALTimetry) project on development of radar altimetry data processing in the oceanic coastal zone (COASTALT 2009; Obligis et al. 2011). A similar approach, the composite correction, has been used by Mercier et al. (2012) and is being implemented in

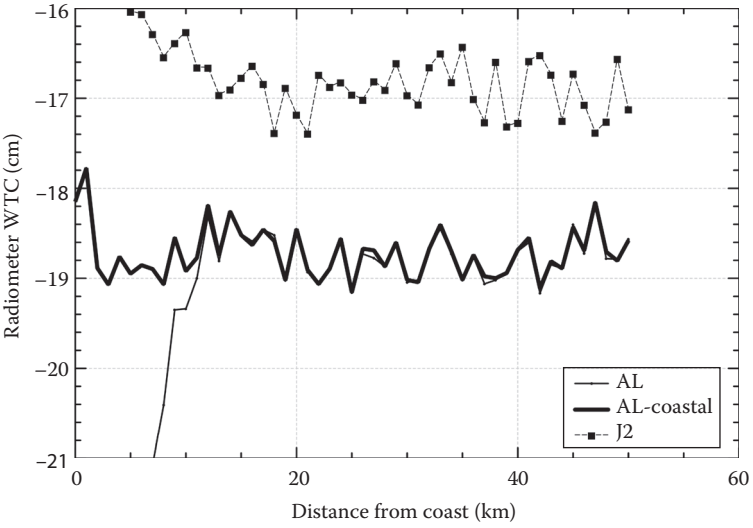

FIGURE 11.5 Wet Tropospheric Correction for AltiKa without any specific coastal processing (thin solid line) and with extrapolation of the last valid ocean brightness temperature (bold solid line). (From Valladeau, G., et al., *Marine Geodesy*, 38(Suppl 1), 124–142, 2015.)

the Archiving, Validation, and Interpretation of Satellite Data in Oceanography (AVISO) products. The composite correction is a conceptually simple method, which consists of replacing the MWR measurements near the coast (less than 50 km) by ECMWF model values. The ECMWF correction is shifted to the nearest valid radiometer measurement in the transition zone. Interpolation and detrending are also applied in complex cases (Mercier et al. 2010).

The Land Contamination Algorithm (LCA) was proposed around the end of the 1990s. This method (Ruf and Giampaolo 1998; Bennartz 1999; Desportes et al. 2007) is based on a correction of the land contamination of the BTs before applying the wet tropospheric correction retrieval algorithm. The correction is generally a function of the land fraction and land surface emissivity in the radiometer footprint. An example is shown in Figure 11.6.

The MPA has been developed at the Jet Propulsion Laboratory (JPL, USA). It is based on the existing open-ocean algorithm for the reference missions but extending to mixed land-ocean scenes, thus enabling retrievals in the coastal zone. It parameterizes log-linear coefficients as a function of the 18.7-GHz land fraction using a database of modeled coastal land BTs. The method requires an accurate land/sea mask and is directly applicable only to missions possessing three-band radiometers, including the 18.7-GHz channel. It has been successfully applied first to Jason-2 data (Brown 2010) and later to Jason 1.

The GPD Plus (GPD+) is the most recent version of the methods developed at the University of Porto to retrieve improved WTC, both for missions carrying an onboard MWR and for missions such as CryoSat-2, which does not possess such an instrument (Fernandes and Lázaro 2016). The GPD+ are wet path delays based on: (1) WTC from the onboard MWR measurements whenever they exist and are valid and (2) new WTC values estimated, by data combination through space–time objective analysis (OA) of all available observation in the vicinity of the estimation point, whenever the previous are considered invalid. Three types of observations have been considered: WTC from valid MWR values, WTC derived from scanning imaging MWR (Si-MWR) onboard various remote sensing missions, and GNSS-derived WTC from coastal and island stations. The underlying

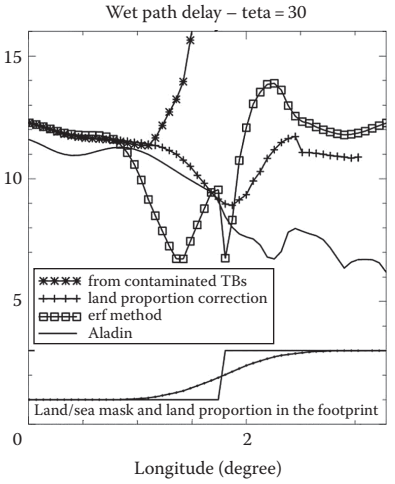

FIGURE 11.6 Wet path delays (in centimeters) on a coastal approach. The two solid lines at the bottom show the land/sea mask (land is on the right) and the land proportion in the radiometer footprint. The lines in the upper part of the figure are the path delays from the contaminated brightness temperatures (crossed solid line, with an unrealistic deviation on approaching the coast), from an analytical correction method ("erf method", line with squares, which also displays a prominent coastal artifact) and from the land contamination algorithm ("land proportion correction"); the latter is closest to the path delay predicted by the ALADIN model (solid line) in the coastal strip. (Reprinted from Desportes, C., et al., *IEEE Trans. Geosci. Rem. Sens.*, 45(7), 2139–2149, 2007. With permission. © 2007 IEEE.)

method, first developed for coastal altimetry in the scope of COASTALT, has been described in Fernandes et al. (2010, 2015) and Fernandes and Lázaro (2016). It improves data retrieval not only near the coast but also in open-ocean, by correcting the baseline MWR-derived WTC from other sources of error (ice and rain contamination and instrument malfunction).

In the scope of the Sea Level CCI project (http://www.esa-sealevel-cci.org) GPD+ WTC have been derived for the main altimetric missions (T/P, Jason-1, Jason-2, ERS-1, ERS-2, Envisat, CryoSat-2, and SARAL/AltiKa) and was later extended to GEOSAT Follow-On (Fernandes and Lázaro 2016). To ensure consistency and the long-term stability of the WTC, the large set of radiometers used in the GPD+ estimations have been inter-calibrated, using as reference the set of Special Sensor Microwave Imager (SSM/I) and SSMI/I Sounder (SSM/IS) on board the DMSP satellite series, due to their well-known stability and independent calibration (Wentz 2013).

The GPD+ corrections have been shown to reduce the sea level anomaly variance with respect to previous versions, to model-derived corrections, and to the AVISO Composite correction. They also have significant impacts in the estimation of regional sea level trends. Improvements are particularly significant in the coastal and polar regions, for T/P, and all ESA missions (Figure 11.7).

The last method developed and tested is based on a one-dimensional variational scheme (1DVAR) to retrieve the wet path delay for altimetry near coasts. This method, one output of which is shown in Figure 11.8, combines radiometric measurements, an *a priori* information on atmosphere (background data provided by ECMWF), and surface emissivity. Contrary to the previously described approaches, the 1DVAR scheme does not directly estimate an integrated content but will retrieve specific humidity and temperature profiles, from which the WTC is eventually computed. The combination of profile estimation and surface emissivity constraint makes this method very flexible and able to handle on-the-fly surface emissivities estimated from the model (e.g., from FASTEM-5, a fast microwave oceanic surface emissivity model over ocean), atlases (Karbou et al. 2005), or retrieved from coincident dedicated channel observations and consequently adapted to every atmospheric situation (standard or above upwelling regions) and surface type (ocean, land, sea ice, hydrology targets, and any transitions).

All these methods have in common handling the contamination on the measured brightness temperatures with coarse spatial resolution in order to retrieve a correction as clean as possible. Then, a new generation of instruments, with smaller footprints and additional atmospheric and surface information, is expected in future altimetry missions (Figure 11.9). In parallel to a classical low-frequency

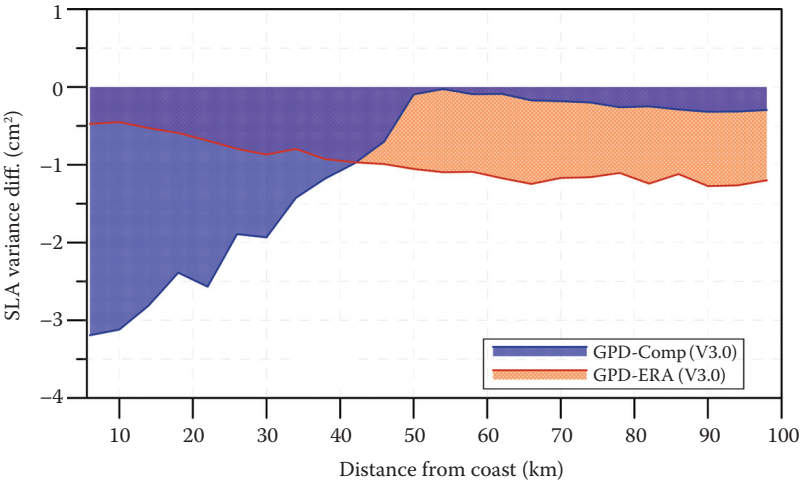

FIGURE 11.7 Variance difference between GPD+ and Composite WTC (blue) and ERA (orange), function of distance from coast, for Envisat MWR Reprocessing V3.0.

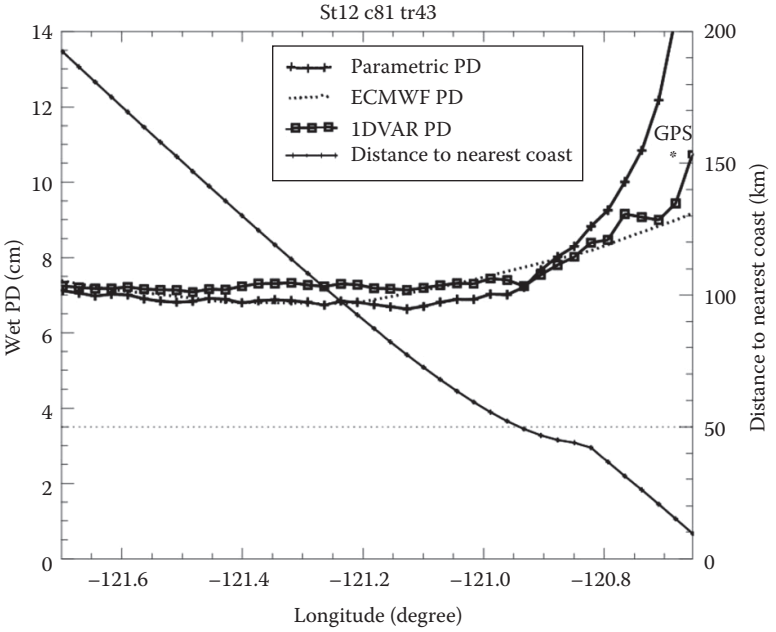

FIGURE 11.8 Wet Tropospheric Correction retrieved with a one-dimensional variational approach (squared solid line), compared with other methods, that is, a parametric approach and the ECMWF model, on a coastal approach. The wet path delay from a Global Positioning System (GPS) coastal station is also shown. (Reprinted from Desportes, C., et al., *IEEE Trans. Geosci. Rem. Sens.*, 48(3), 1001–1008, 2010. With permission. © 2010 IEEE.)

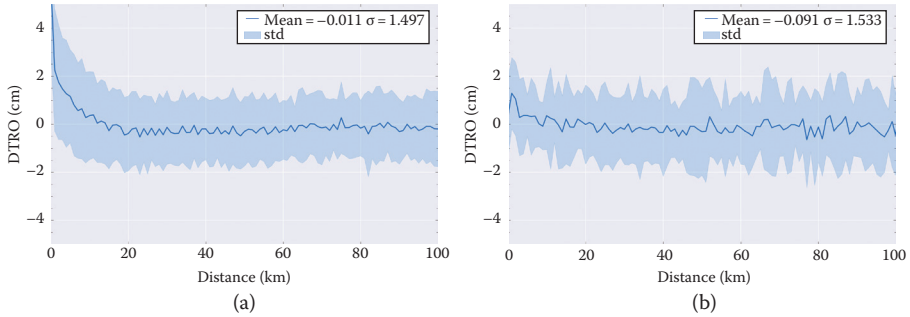

FIGURE 11.9 Difference between the retrieved Wet Tropospheric Correction (WTC) from a combination of (89 Hz + 157 GHz + 183.3 GHz) channels from Microwave Humidity Sounder (MHS) and the ECMWF WTC, as a function of along distance to coast over the Mediterranean Sea. (a) Neural network: The land contamination occurs shoreward of 20 km as shown by the increase in the correction difference; (b) 1DVAR approach: The land contamination is clearly reduced (Credit: ACCRA ESA study).

channel with a spatial resolution of about 30 km, the radiometers would embark a set of high-frequency channels, with footprints of about 10 km. Typical observation frequencies would be 50 GHz dedicated to surface emissivity and atmospheric temperature, 89 GHz dedicated to cloud content, and 183 GHz dedicated to both water vapor and cloud content.

In conclusion, the future of the WTC on coastal regions relies on a new generation of microwave radiometers and dedicated retrieval algorithms ready to take advantage of additional information on surface, atmospheric temperature and humidity, and cloud content.

11.3.3 Recent Improvements in Coastal Tides and Dynamic Atmospheric Correction

The standard altimetry corrections corresponding to the tides, to the changing atmospheric pressure (i.e., inverted barometer effect), and to the high-frequency atmospheric forcing are provided by global models. These geophysical effects tend to be much larger, complex, and associated with shorter wavenumbers in shelf and near-coastal waters than in deep waters. It places a critical demand on the accuracy of the corresponding numerical solutions (Andersen and Scharroo 2011). As a consequence, different groups worldwide have devoted substantial efforts to improving correction models and algorithms in coastal regions. The high-frequency dynamic ocean response to atmospheric forcing provided by the Toulouse Unstructured Grid Ocean (T-UGO) model hydrodynamic finite element model (Carrère and Lyard 2003), which is an evolution of the widely used MOG2D (Modèle aux Ondes de Gravité—two dimensions) is now commonly added to the inverted barometer correction. Considerable efforts have been oriented to improve spatial model resolution, numerical schemes, realism of the underlying hydrodynamic models and data assimilation techniques, better knowledge of the local near-coastal bathymetry and coastlines, developing regional models, and assembling independent data sets for the validation. Regular exercises of tidal model inter-comparisons (as in Stammer et al. 2014) highlight that much progress has been achieved in global tidal solutions. Significant differences are still observed in some coastal areas, such as the Amazonian shelf, the Indian Ocean, and the Indonesian region, where the recent FES2014 tidal atlas (the most recent release of a series of global finite element tidal solutions initiated by Le Provost et al. 1994) appears to be the most accurate (Birol et al. 2016). In parallel, modeling individual coastal regions has proven to offer additional progress for both the tidal and atmospherically forced high-frequency corrections (Roblou et al. 2011). Regional model corrections based on the T-UGO 2D hydrodynamic code are now available over an increasing number of coastal seas (Maraldi et al. 2007; Pairaud et al. 2008; Le Bars et al. 2010). This correction issue continues to be at the forefront of current research, and we can expect to see further important progress in the coming years.

11.4 DATA AVAILABLE FOR COASTAL ALTIMETRY

Several projects have been and are generating data with algorithms tuned for the coastal zone, and data are provided at a higher post rate (20 Hz or 40 Hz, corresponding to along-track distances of approximately 350 and 175 m, respectively), which makes them more amenable to coastal altimetry applications. Table 11.1 (from Cipollini et al. 2017) summarizes the main characteristics of the available products. The following subsections provide more information on three specific products (i.e., PEACHI, ALES, and X-TRACK), highlighting their main characteristics.

11.4.1 PEACHI Expertise Prototype

With the objective to ensure the complementarity but also the continuity with the Level-2 S-GDR products provided in the open ocean, the Prototype for Expertise on Altimetry for Coastal, Hydrology and Ice (PEACHI) project has been set up as an initiative of the French space agency, CNES. The PEACHI prototype is designed not only to serve coastal applications but is also considered as a reference to compute and provide dedicated algorithms over ice regions and for hydrological studies. The PEACHI project thus focuses on a handful of key algorithm improvements with regard to the operational Geophysical Data Record (GDR) products. The main objectives of the prototype are the following:

1. Validate and implement the existing algorithms before their application in the operational products.
2. Develop new algorithms linked to scientific objectives (coastal areas, surface hydrology, rain cells, continental and sea ice, etc.).
3. Ensure both complementarity and continuity with the altimeter measurements over the open ocean.

TABLE 11.1
Available Coastal Altimetry Products as of July 2017

ID	Produced by	Altimeter	Product level	Posting rate	Coverage	Download from	Comments
PISTACH	CLS CNES	j2	L2	20 Hz	Global	AVISO+	Experimental Jason-2 products for Hydrology and Coastal studies with specific processing. Will be discontinued at the end of 2016 in favor of PEACHI
PEACHI	CLS CNES	sa, (j2 to be added soon)	L2	40 Hz	Global	AVISO+ / ODES	Experimental SARAL/AltiKa products including dedicated retracking and corrections leading to more accurate products for coastal zones, hydrology and ice. From 2017 expected to generate also j2 products
XTRACK	LEGOS-CTOH	tx, j1, j2, gfo, en (sa to be added soon)	L2, L3	1 Hz 20 Hz (test)	23 regions covering the whole coastal ocean	CTOH AVISO+ / ODES	Specific processing using improved data screening and latest corrections available
ALES	NOC	j2, n1, (j1, j3 to be added soon)	L2	20 Hz	Global, <50 km from coast	PODAAC	Experimental products from the ALES processor included in SGDR-type files alongside the standard products and corrections.
SARvatore	ESA-ESRIN	c2 (SAR only)	L2	20 Hz	SAR mode regions	ESA G-POD	On-demand Processing service for the CryoSat-2 SAR mode data where the user can configure some processing parameters to meet specific requirements (for instance for the coastal zone)
COP	ESA	c2 (LRM/ PLRM)	L2	20 Hz	Global	ESA	Global products for CryoSat-2 from an Ocean processor (output is in PLRM over the SAR mode regions) - but no specific coastal processing
COSTA	DGFI-TUM	e2, en (other altimeters available on request)	L3	1 Hz 20 Hz	Mediterranean and North Sea (other regions available on request)	PANGAEA	Dedicated coastal altimetry sea level measurements based on enhanced ALES retracker

Note: The abbreviations used for the altimeters are e1: ERS-1 (1991-1996); tx: TOPEX (1992-2002); e2: ERS-2 (1995–2011); gfo: GEOSAT Follow-On-1 (2000–2008); j1: Jason-1 (2002–2013); n1: Envisat (2002–2012); j2: Jason-2 (2008–present); c2: CryoSat-2 (2010-present); sa: SARAL/AltiKa (2013–present); j3: Jason-3 (2016–present). For CryoSat-2 (c2), a further specification is added when data are only available from the Low-Resolution Mode and Pseudo-Low Resolution Mode (LRM/PLRM) or only from the Synthetic Aperture Radar (SAR) mode regions. The abbreviations used for product levels are L2: along-track data with corrections; L3: data projected on regularly spaced reference points along the nominal ground tracks of the satellite. From Cipollini et al. (2017), with additions, available under the terms of the Creative Commons Attribution 4.0 International License.

11.4.1.1 SARAL/AltiKa

The PEACHI Expertise Prototype was first initiated with the SARAL/AltiKa space mission launched in 2013. The main objective of the SARAL/AltiKa mission is to better observe the open ocean, but the mission is also targeting secondary objectives, such as the study of coastal dynamics. The prototype has been designed to complement SARAL/AltiKa processing software and the dissemination of the operational Level-2 products with some new or improved algorithms and therefore to analyze and improve processing dedicated to the Ka-band radar altimeter (Valladeau et al. 2016).

Over coastal regions, the prototype aims to provide end users with new waveform retrackers, a geometrical waveform classification, improved two-dimensional and new three-dimensional SSB, new tide models, better altimeter wind correction and a new wet troposphere correction (Valladeau et al. 2015).

Figure 11.10 displays the standard deviation of the altimeter range with regard to the distance from the coast. Compared to Jason-2, better performances were expected for SARAL/AltiKa close to the coasts, thanks to 40 Hz sampling and a smaller waveform footprint. These improvements are due to AltiKa's larger bandwidth, lower orbit, increased pulse repetition frequency (PRF), and reduced antenna beamwidth (Steunou et al. 2015). Real measurements confirm these expectations with an excellent behavior of SARAL/AltiKa closer to the coast in terms of standard deviations of the range, significant wave height, and sigma naught. Until 5.7 km off the coast, the standard deviation of the range remains stable for AltiKa (lower than 10 cm), while it increases for Jason-2 close to 10 km from the coast. Note that differences in the level of standard deviations in the open ocean originate in the temporal sampling of both altimeter missions (40 Hz for SARAL and 20 Hz for Jason-2).

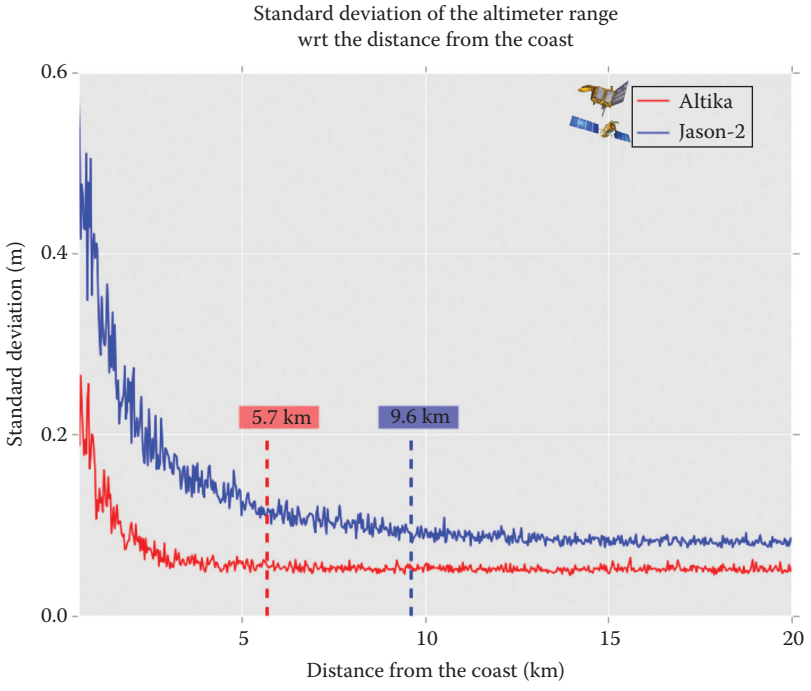

FIGURE 11.10 Performance of SARAL/AltiKa and Jason-2 altimeters near the coast: standard deviation of the altimeter range with respect to the distance from the coast. AltiKa (red curve) is remarkably more precise. (From Cipollini, P., et al., *Surv. Geophys*., 38, 33, 2017.) Available under the terms of the Creative Commons Attribution 4.0 International License.

TABLE 11.2
List of PEACHI SLA Products Available and the First and Last Dates of the Time Series

Mission	Start	End
SARAL/AltiKa	03/14/2013 (1)	07/04/2016 (35)
SARAL/AltiKa drifting orbit	07/04/2016 (100)	12/26/2016 (104)
Jason-2	12/27/2014 (239)	10/02/2016 (303)
Jason-2 interleaved	10/13/2016 (305)	12/15/2016 (311)

Note: The corresponding cycle number is indicated in parentheses.

11.4.1.2 Implementation on Jason-2 and Jason-3

The PEACHI Expertise Prototype has been designed to serve multiple altimeter missions with a homogenous processing sequence and thus corresponding data sets provided to the end users. Therefore, the PEACHI prototype is also computed on-the-fly for the Jason-2 and Jason-3 missions, and the same panel of algorithms are computed as for SARAL/AltiKa for better cross-comparisons over coastal regions. On Jason-2, the prototype replaces the PISTACH Prototype released in 2009 (Dufau et al. 2011). Concerning Jason-3, the PEACHI-J3 experimental processing prototype is delivering delayed-time products to the expert users' community. PEACHI-J3 products are based on S-(I)GDR Jason-3 official products, enriched with specific algorithm outputs such as numerical retracking estimates, new wet tropospheric correction, and other useful corrections such as three-dimensional SSB correction and updated geophysical corrections.

11.4.1.3 Data Availability and Delivery Mode

PEACHI products are made from S-GDR altimeter products with specific processing (improvements of conventional satellite radar altimetry parameters lead to more accurate products over several surface types: open ocean, coastal regions). Constantly seeking to address its users' needs, AVISO+ proposes new features and products for its dissemination service called Online Data Extraction Service (ODES, http://odes.altimetry.cnes.fr) in order to provide users and applications with a wider range of altimetry-derived data and services. The summary of the products currently available is in Table 11.2.

11.4.2 ALES

11.4.2.1 ALES Data Set: Availability and Reliability

The ALES retracking algorithm (see Section 11.2.1) has already been implemented for Jason-1, Jason-2, ERS-2, Envisat, and SARAL/AltiKa, while the adaptation to Jason-3, CryoSat-2 Low Rate Mode, and ERS-1 is under development and validation.

Currently, Envisat and Jason-2 ALES data sets have been made freely available in the global coastal ocean (see Table 11.3), between 0 and 50 km from the coastline, distributed by the Physical Oceanography Distributed Active Archive Center (PO.DAAC) through the portal https://podaac.jpl.nasa.gov/data set/ALES_L2_OST_JASON2_V1. The data format follows the original Sensor Geophysical Data Record (SGDR): Range, Significant Wave Height (SWH), and Backscatter Coefficient (Sigma 0) estimated from ALES are available along every track together with the standard altimetry products. By combining the ALES Range estimates with the corrections needed to extract the sea level height (see Section 11.3), the user can analyze coastal sea level anomalies that are usually reliable up to 3 km from the coast (Passaro et al. 2014).

TABLE 11.3
List of ALES Products Available from PO.DAAC and the First and Last Dates of the Time Series

Mission	Start	End
Jason-2 GDR-D	07/21/2008 (2)	05/15/2015 (252)
Envisat-v2.1	05/14/2002 (6)	10/21/2010 (94)

Note: The corresponding cycle number is indicated in parentheses. Further products based on the ALES algorithm are now becoming available from the COastal Sea level Tailored ALES (COSTA) Project at https://doi.pangaea.de/10.1594/PANGAEA.871920 (see Table 11.1).

The ALES range has been validated by means of comparison with tide gauges in terms of correlations and root-mean-square (RMS) errors in different regions, including in bays with jagged coastlines such as the Gulf of Trieste (Passaro et al. 2014) and the Strait of Gibraltar (Gómez-Enri et al. 2016), showing consistent improvements. As an example, comparing Jason-1 track 161 with the Trieste tide gauge at the along-track location closest to the gauge (approximately 5 km from the coast), the ALES time series has a correlation coefficient of 0.93 with the time series extracted from the gauge at the times of the altimeter overpasses, as opposed to 0.60 for the standard product. Also, the SWH estimations have been validated against buoys in the German Bight: Improvements in terms of correlation are seen up to more than 20 km within the coast, while the noise of the high-rate SWH retrieval is steadily less than in the standard products (Passaro et al. 2015b).

The future objective of the ALES project is the distribution of averaged coastal sea level anomalies (i.e., a Level 3 product) by combining the ALES retracking with a new SSB correction, a post-processing based on outlier detection, and a set of up-to-date external geophysical corrections.

11.4.2.2 ALES Data Set Improves Coastal Sea Level Research

Figure 11.11 shows an example of the improvement that it is possible to obtain in terms of data quality and quantity with ALES compared to an altimetry data set that has been designed for the open ocean, such as the ESA Sea Level Climate Change Initiative (SL_cci) data set (http://www.esa-sealevel-cci.org/products). In the figure, each 1-Hz point of the North Sea/Baltic Sea intersection zone corresponds to the standard deviation (std) of the 2002–2010 sea level computed from Envisat in the specific location. The ALES product shows smooth variations of the std, with the exception of a few locations: No abrupt change is to be expected, given that consecutive points are spaced by roughly 7 km. This is not verified in the SL_cci, which is not tailored for coastal exploitation, and signs of corrupted estimations are evident in the unrealistically high std of several 1-Hz locations. The reliability of ALES in comparison to standard altimetry products, such as SL_cci and the Radar Altimetry Database System (RADS), is evident from the histogram in Figure 11.12, in which the ALES statistics of the RMS of the time series at each 1-Hz point of the same area of study show almost no outliers.

In the same region, the ALES Envisat product has been used to perform a sub-regional analysis of the sea level annual variability. The reliability of the data set has been verified by direct comparison to the annual signal estimated from the seven tide gauges (TGs) in the same area (Table 11.4). These differences demonstrate that the ALES estimates are more similar to the TG results than the corresponding values from standard altimetry products (SL_cci and RADS).

The availability of coastal estimates of SWH and backscatter coefficients is allowing the recomputation of the SSB correction in the coastal ocean (see Section 11.4.3), which is one of the main

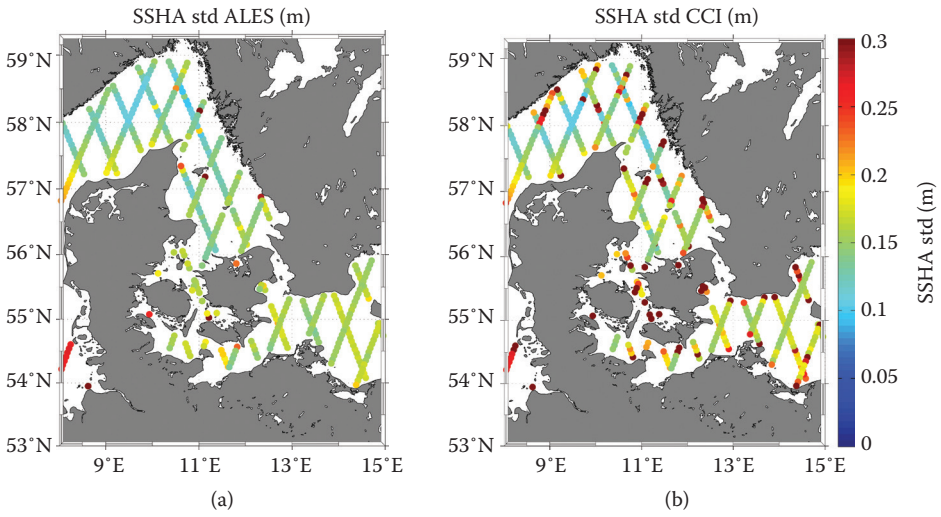

FIGURE 11.11 North Sea/Baltic Sea intersection: Comparison between (a) ALES reprocessed and (b) SL_cci data sets in terms of standard deviation of the Envisat SSHA time series (2002–2010) for each 1-Hz location. (Reprinted from Passaro, M., et al., *J. Geophys. Res. Oceans*, 120(4), 3061–3078, 2015a. With permission. © 2015 American Geophysical Union.)

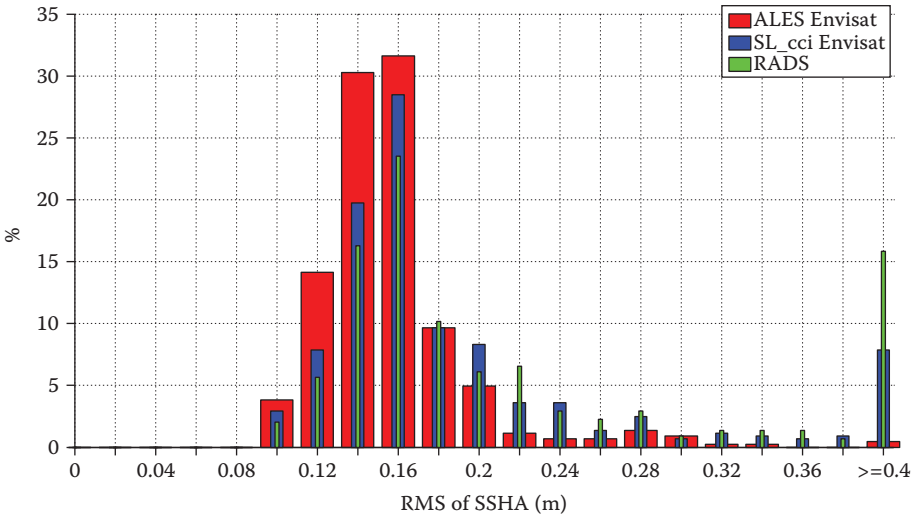

FIGURE 11.12 Histogram of the root mean square of SSHA computed at each 1-Hz location in the North Sea/Baltic Sea intersection from ALES reprocessed (red), Envisat SL_cii (blue), and Radar Altimetry Database System (RADS; green) data sets. Reprinted from Passaro, M., et al., *J. Geophys. Res. Oceans*, 120(4), 3061–3078, 2015a. With permission. © 2015 American Geophysical Union.)

sources of uncertainty in coastal altimetry. The SSB correction in the standard products is based on an empirical function of SWH and wind (derived from the backscatter coefficient estimated by the retracking). Preliminary studies along the coast of Spain have shown that the use of this relation with the ALES SWH and wind estimates leads to a reduction of the along-track coastal SLA uncertainty by up to 25% (Gómez-Enri et al. 2016).

TABLE 11.4
Root-Mean-Square (RMS) Difference between the Sinusoids Corresponding to the Annual Cycle of the Sea Level Estimated by the Tide Gauges and the Sinusoids Estimated from Different Altimetry Data Sets for Each Sub-Basin of the North Sea/Baltic Sea Intersection Zone (Data from Envisat 2002–2010)

SUBBASIN	ALES (m)	SL_cci Env (m)	RADS (m)
Kattegat	0.012	0.019	0.023
Norway Skagerrak	0.014	0.022	0.028
Denmark Skagerrak	0.008	0.008	0.012
Sweden Skagerrak	0.008	0.010	0.013
West Arkona	0.004	0.031	0.024
East Arkona	0.005	0.016	0.773
Belts	0.006	0.008	0.027

Source: Reprinted and reformatting from Passaro, M., et al., *J. Geophys. Res. Oceans*, 120(4), 3061–3078, 2015a. With permission. © 2015 American Geophysical Union.

11.4.2.3 Examples of Usage of the ALES Data Set

The ALES data set has been used to provide a sea level advice service to support agencies responsible for planning coastal flood defenses in the United Kingdom in the framework of the Sea Level Space Watch program (Cipollini and Calafat 2016), producing maps of trends and seasonal variability that show significant regional differences and highlighting the still crucial effect of the choice of tidal models in the coast.

ALES was also chosen in the ESA eSurge project (http://www.storm-surge.info) to observe the development of storm surges in the coastal ocean: As a case study, Cyclone Hagupit was captured by Jason-2 on May 12, 2014, and ALES reprocessed data revealed a clear bulge of SSHA at the storm's center (Harwood 2015).

More results of the oceanographic studies based on ALES are discussed in Section 11.6.

11.4.3 X-TRACK Regional Altimetry Products

A different approach than waveform retracking was adopted by Laboratoire d'Études en Géophysique et Océanographie Spatiales (LEGOS) who concentrated on the post-processing step and developed a data-editing algorithm able to look for the best trade-off between the quantity and the quality of altimetry observations over marginal seas. This software, called X-TRACK (Roblou et al. 2011; Birol et al. 2016), analyzes the behavior of the different altimeter corrective terms as a whole and then edits and recomputes the suspicious correction values with the aim of maximizing the number of useful near-shore sea level data finally available for the user. It is now routinely operated at the Center for Topographic studies of the Ocean and Hydrosphere (CTOH, French observation service dedicated to satellite altimetry studies), and a large part of the archive of altimetry data has been reanalyzed. X-TRACK regional products are freely distributed (http://ctoh.legos.obs-mip.fr/products/coastal-products/ and http://www.aviso.altimetry.fr/en/data/products/sea-surface-height-products/regional/x-track-sla.html), providing Level 3 along-track sea level anomaly (SLA) products from different altimetry missions for coastal and regional applications. Some products combine the observations from different missions that are on the same orbit. They are all computed in the same way, resulting in coherent multi-mission data sets, which is particularly important for climate

research. Table 11.5 indicates the 1-Hz SLA products available and, for each, the first and last dates of the time series. Together with mono-mission products (T/P+ T/P interleaved, Envisat, GFO, Jason-1 + Jason-1 interleaved, and Jason-2) users can retrieve SLA for T/P + Jason-1 + Jason-2 and T/P interleaved + Jason-1 interleaved combined missions. The processing is done on a regional basis and, in parallel to the altimeter missions, the areas covered by X-TRACK regional products have progressively increased since 2007, and now include all the coastal oceans (Figure 11.13).

For each region, both raw and along-track low-pass filtered (using a 40-km cutoff frequency) 1-Hz SLA time series along the nominal ground tracks are available. They are provided together with: (1) an along-track mean sea surface height profile based on the data over the largest whole number

TABLE 11.5
List of X-TRACK SLA Products Available and the First and Last Dates of the Time Series

Mission	Start	End
TOPEX/Poseidon (T/P)	02/28/1993 (17)	08/12/2002 (364)
Jason-1 GDR-C	01/15/2002 (1)	01/27/2009 (259)
Jason-2 GDR-D	07/12/2008 (1)	05/26/2016 (290)
T/P+Jason-1+Jason-2	02/28/1993 (17 of T/P)	05/26/2016 (290 of Jason-2)
T/P interleaved	09/21/2002 (369)	10/09/2005 (481)
Jason-1 interleaved	02/10/2009 (262)	02/15/2012 (372)
Envisat-v2.1	10/01/2002 (10)	09/14/2010 (92)
GEOSAT Follow-On (GFO)	01/08/2000 (37)	09/08/2008 (222)
T/P interleaved+Jason-1 interleaved	09/21/2002 (369 of T/P)	02/15/2012 (372 of Jason-1)

Note: The corresponding cycle number is indicated in parentheses.

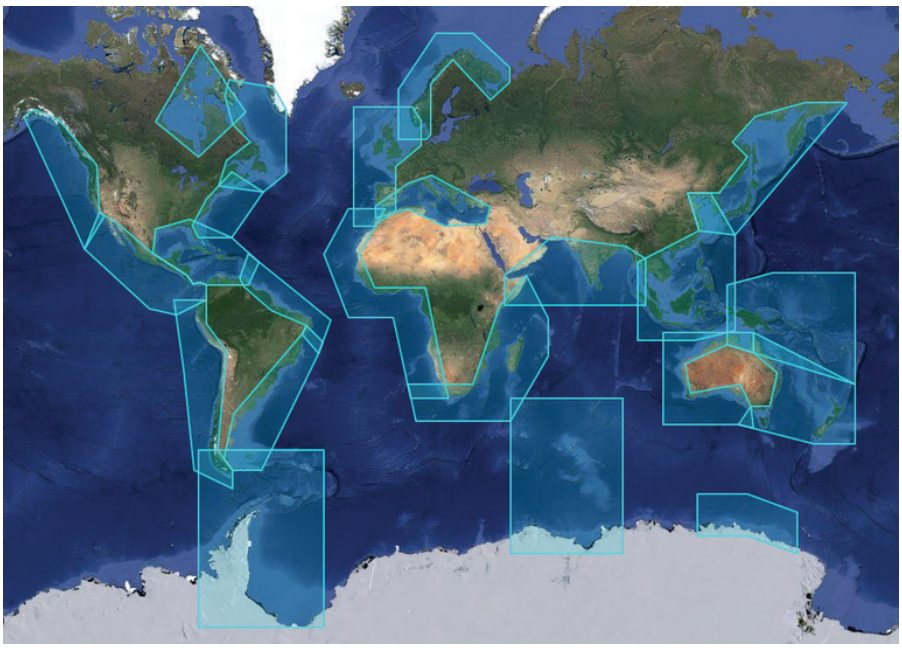

FIGURE 11.13 Map of X-TRACK regional products in 2016.

of years covered by the SLA data, (2) the tidal and dynamical atmospheric correction (DAC) used (applied to SLA data but provided for specific applications), (3) the distance to the nearest coast (in 2016, computed from the NOAA product at a spatial resolution of 0.04°, http://oceancolor.gsfc.nasa.gov/DOCS/DistFromCoast/), and (4) the mean dynamic topography (MDT).

The historical X-TRACK processing methodology is described in Vignudelli et al. (2005) and Roblou et al. (2011). It is continuously evolving and the editing strategy has been entirely revisited in the 2016 version. If the general principle remains the same, each altimetry corrective term is now edited in a different way in order to take into account its individual characteristics (i.e., the corresponding geophysical variations along the track; for more details, see Birol et al. 2016). It was shown to result in higher correlations between coastal altimeter and tide gauge sea level anomalies (by 15% in average) compared with the previous version of the algorithm. The suitability of the X-TRACK approach was shown in different regional studies, where compared to the operational AVISO processing algorithm, it results in a significant increase in the quantity of available data near coastlines (Vignudelli et al. 2005; Durand et al. 2008, Birol et al. 2010; Melet et al. 2010, Passaro et al. 2014; Jebri et al. 2016). For example, Birol et al. (2016) showed that along Western Africa, sea-level variations derived from X-TRACK data are observed closer to land (5 km) compared to AVISO (10 km). Sea-level statistics are more robust due to the larger and more stable data availability (Cipollini et al. 2016), and this leads to an improved observation of the near-shore ocean dynamics in different regions, in particular the boundary circulation (Durand et al. 2008, Birol et al. 2010; Bouffard et al. 2011; Liu et al. 2012; Jebri et al. 2016).

The improvement of the coastal altimetry SLA data has led the CTOH to also derive the empirical harmonic constants (amplitude and phase lags) for a number of tidal constituents by using harmonic analysis (Birol et al. 2016). The tidal constants database is computed using the 1-Hz SLA time series processed by X-TRACK, taking advantage of the T/P, Jason-1, and Jason-2 long time series. It is also distributed on a regional basis. The files hold the along-track estimates of amplitude and phase for a number of tidal constituents (see Table 11.3 of Birol et al. 2016) and two along-track error estimates associated with the tidal constants: (1) a formal error computed from the inverse method theory and (2) an error accounting for the ocean background signal associated to aliased tidal frequencies.

All these products are validated before distribution. Comparisons with Level 3 AVISO products and a number of tide gauge records are made for the 1-Hz SLA. Altimetry tidal constants are systematically compared to global model solutions. Many of the corresponding diagnostics are available on the CTOH web site. A new release of the products is proposed every year (including longer time series, new developments, new altimeter missions, etc.). A specific digital object identifier (DOI) has been created to identify X-TRACK products: 10.6096/CTOH_X-TRACK_2015_01. Finally, X-TRACK is not only a product but also a data service. It has been developed considering the input from users, and specific data sets can be computed on request for particular applications. This is important because no consensus exists yet concerning standard coastal altimetry processing and products—this is something on which the community of developers and users of coastal altimetry will hopefully converge in the next few years.

11.5 APPLICATIONS USING OBSERVATIONS ALONE

The oceanographic applications that are made possible or improved in coastal domains by the use of altimeter data are primarily those that require information about sea level and surface currents. A smaller number of applications use estimates of surface wave heights along altimeter tracks (for instance, Passaro et al. 2015b), while very few use altimeter estimates of wind speed. The fact that wind and wave conditions change more rapidly (in hours to a day) than circulation features may explain their lower rate of use along altimeter tracks, which are widely spaced over several hundred kilometers and 10–35 days. Meteorological buoys and atmospheric models provide wind estimates every 1–4 h; these winds, in turn, are used to force wave models. Those relying on frequent updates of wind and wave conditions,

including forecasts, use the model fields. The sparse altimeter observations are more likely to be used to validate model wave and wind forecasts or to look at specific events in retrospective studies.

SSH and SLA fields over the ocean, however, are the unique contribution of altimeters. Coastal tide gauges, bottom pressure sensors, and inverted echo sounders can provide more rapid and complete time series at select points, but only altimeters provide data with enough coverage to create gridded time series of two-dimensional surface height fields on weekly to monthly timescales. Geostrophic currents, calculated from the height gradients, are also available over the global coastal ocean with coverage unobtainable from other sources, either as cross-over vector velocities, cross-track components of velocity, or as gridded fields.

Applications that combine altimeter data with numerical and statistical models are discussed in the next section. Here we consider applications that use observations without models, either from one or more altimeters by themselves or in combination with other satellite and *in situ* data sets. Our consideration of applications can also be divided spatially into those that consider the large-scale boundary currents (extending several hundred kilometers offshore) and others that are confined to the narrower region within several tens of kilometers of land—even extending onshore to quantify river discharge and coastal inundation.

Previous reviews of ocean remote sensing include coastal and fisheries applications in the large-scale boundary currents. Although most of these use sea surface temperature (SST) and ocean color, a few utilize altimeter data. Mitchum and Kilonsky (1995) compare altimeter measurements of sea level variability to tide gauge measurements, connecting inherently coastal observations to large-scale oceanography. Ikeda and Dobson (1995) discuss early retrievals of surface waves and winds from altimeters, although not in coastal contexts. Janssen (2000) and Atlas and Hoffman (2000) discuss altimeter wave and wind measurements over the open ocean. Garzoli and Goni (2000) provide altimeter-derived transport estimates in boundary currents (the Agulhas and Benguela). Oliveira et al. (2000), while looking at the movement of meddies (salty lenses of Mediterranean water), also use along-track altimeter data to characterize these large-scale eddies, which pass near the eastern boundary current next to the Iberian Peninsula. Reynolds et al. (2000) present an early example of assimilation of altimeter data into a large-scale ocean model that simulates the 1997 to 1998 El Niño, the topic of the next section. The more recent review of "Oceanography from Space" by Barale et al. (2010) describes applications of altimeter data for large-scale ocean circulation and sea level, MDT, the marine geoid, and planetary waves. Although coastal regions are not discussed per se, these discussions provide the background and underlying basis for coastal applications.

Vignudelli et al. (2011) present the first comprehensive review of the use of altimetry in coastal regions and discuss regional applications of altimeter-derived fields (primarily coastal currents and sea levels) in the northwest Mediterranean Sea; the Caspian Sea; Black Sea; Barents and White Seas; the coasts of North America; China's coastal seas; Australia; and in lakes in South America, East Africa, and Asia. For publications since 2011, the reader is directed to the literature databases maintained at NASA's Jet Propulsion Laboratory for the Ocean Surface Topography Science Team (search "sealevel.jpl.nasa.gov" under "Science" and "Literature Database") and for the Surface Water, Ocean Topography Science Team (search "swot.jpl.nasa.gov" under "Science" and "Publications" as well as under "Applications"). Presentations from a series of Coastal Altimetry Workshops held since February 2008 can also be found on the COASTALT Website (http://www.coastalt.eu).

Over the longest timescales, decadal studies of sea level rise from altimeter data depict global maps of the basins, showing the spatial structure of the rising seas (Nerem et al. 2010; Stammer et al. 2013; Ablain et al. 2015). For instance, the eastern North Pacific has a low value of increased sea level (some regions are even decreasing), while the western tropical Pacific is rising faster than the mean rate. Combinations of altimeter and tide gauge data have been used to extend these reconstructions, depicting the global patterns of sea level rise over the past 50 years (Church et al. 2004; Church and White 2006; Hamlington et al. 2011; Meyssignac et al. 2012). More regional studies of sea level rise/change have also been published for the Mediterranean Sea (Calafat et al. 2009), the Indian Ocean (Han et al. 2010), Europe (Feng et al. 2013), the Pearl River Delta (He et al. 2014),

Malaysia (Luu et al. 2015), and the Bay of Biscay (Marcos et al. 2007). An issue related to sea level rise is the vertical movement of the coastal land (Wöppelmann and Marcos 2016). Altimeter data are combined with tide gauges, Global Positioning System (GPS), and other data to investigate vertical land motion in a number of locations (see Wöppelmann and Marcos 2016), including Taiwan (Chang et al. 2012) and the coast of Turkey (Yildiz et al. 2013).

On seasonal timescales, new estimates of spatial and temporal variability in the seasonal cycles of coastal sea level have been published for the northwest Pacific by Feng et al. (2015) and the southwest Atlantic by Ruiz Etcheverry et al. (2016). A common finding on seasonal and shorter timescales is that tide gauges produce more energetic signals than standard altimeter fields. This problem has been addressed by the use of the reprocessed ALES coastal along-track data to derive seasonal cycles of sea level for the North Sea/Baltic Sea intersection zone (Passaro et al. 2015a) and the Indonesian Seas (Passaro et al. 2016, also using CryoSat-2 SAR data). In both regions, the use of ALES data reveals the higher amplitude of annual cycles of the sea level in the presence of coastal currents: the Norwegian Coastal Current in the Skagerrak Sea (Passaro et al. 2015a) and the Java Coastal Current south of Java (Passaro et al. 2016). In the first case, ALES data filled the gap between the higher annual amplitude (approximately 9 cm) registered by a coastal tide gauge and the lower amplitude in the open sea (approximately 4 cm), showing a gradient of annual amplitude that follows the bathymetry slope within 30 km of the coast. In the latter study, it was possible to detect the semiannual Kelvin Wave traveling from the Indian Ocean into the internal seas of Indonesia.

Moving from sea level to studies of regional ocean circulation, an overview of methods of estimating surface currents from satellite data, including altimetry in coastal regions, is given by Klemas (2012). Regional studies of shelf-slope circulation constitute some of the most common applications of coastal and boundary current altimetry, as represented by examples from the Bay of Biscay (Herbert et al. 2011), the northwest Mediterranean Sea (Bouffard et al. 2012), the eastern Gulf of Mexico and West Florida Shelf (Liu et al. 2012, 2014), the southern Bay of Bengal (Wijesekera et al. 2015), and the Agulhas Current (Krug and Tournadre 2012; Krug et al. 2014). In some regions—for example, the southwest Atlantic study of Strub et al. (2015)—fields of MDT are added to the SLA data to calculate absolute geostrophic circulation. The MDT fields may be global (Rio et al. 2014a) or specialized regional MDT fields, such as in the Mediterranean Sea (Rio et al. 2014b). Improvements in the tidal models used to correct the altimeter data are indicated by the fact that some of the aforementioned studies (e.g., Strub et al. 2015) succeed in using standard processed altimeter data over the wide continental shelf.

On synoptic scales of days to weeks, many coastal regions are affected by offshore eddies, as in the case of the meddies (Oliveira et al. 2000) and Agulhas eddies (Garzoli and Goni 2000) noted earlier. An altimetric survey of mesoscale eddies in the global ocean is reported in Chelton et al. (2011b) and is extended to examine the impact of eddies on satellite-derived fields of surface chlorophyll pigment concentrations in Chelton et al. (2011a). Mechanisms by which winds interact with eddies to create patterns of upwelling and downwelling are further explored in Gaube et al. (2015). These same mechanisms apply in both open and coastal ocean regions. One of the more comprehensive descriptions of surface and sub-surface characteristics of eddies in the ocean's major eastern boundary currents is that of Pegliasco et al. (2015), combining altimeter and sub-surface float data. Other descriptions of eddy characteristics and eddy kinetic energy are presented by Bouffard et al. (2012) in the northwest Mediterranean and Caballero et al. (2008) in the Bay of Biscay.

Investigations of the velocity fields next to the coast often use the specially processed data sets described in Section 11.5. This allows analyses to reach closer to the coast and also recovers some of the more energetic signals revealed by tide gauges in comparison to standard altimeter processing. Examples of the use of ALES data to resolve more energetic seasonal cycles of sea level and velocities are presented earlier. On the shorter synoptic scales, X-TRACK regional altimetry products have been used in a wide range of applications: coastal ocean circulation, mesoscale dynamics, hydrodynamic and tidal model validation, tides, development, or validation of new altimeter processing methods (Vignudelli et al. 2005; Durand et al. 2008; Birol et al. 2010; Melet et al. 2010; Bouffard et al. 2011; Liu et al. 2012; Passaro et al. 2014; Birol et al. 2016; Jebri et al. 2016). Figure 11.14 presents the

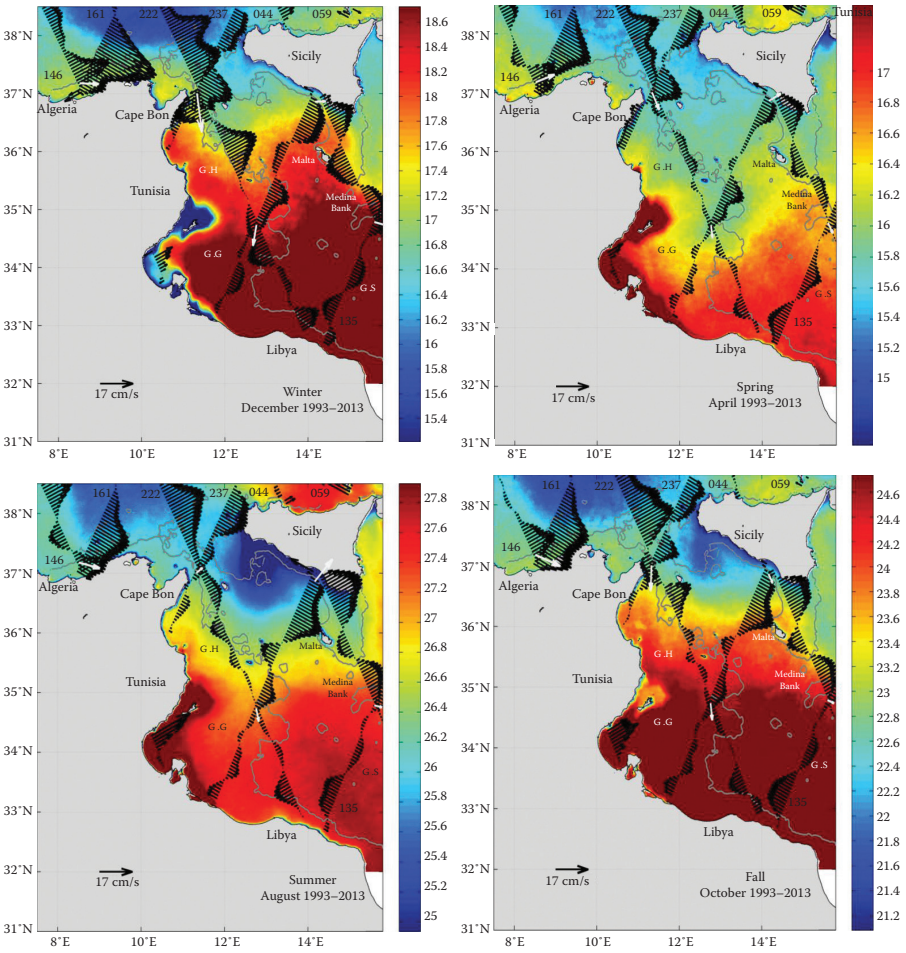

FIGURE 11.14 Maps of cross-track (black) and crossover (white) geostrophic currents for X-TRACK and SST over the climatological cycle. The 200-m isobath (gray solid line) is from the ETOPO2v1 global gridded database. SST data are from the German Aerospace Center (DLR) product with 1.1-km resolution. G.H. is the Gulf of Hammamet, G.G. is the Gulf of Gabes, and G.S is the Gulf of Sirte. (Reprinted from Jebri, F., et al., *J. Geophys. Res. Oceans*, 121(7), 4888–4909, 2016. With permission. © 2016 American Geophysical Union.)

example of the surface circulation over the central Mediterranean Sea observed in Jebri et al. (2016) from X-TRACK altimetry data and remotely sensed sea surface temperature (SST) observations. In this study, after a comparison between altimeter and *in situ* observations, the seasonal evolution of the surface circulation was analyzed in details. The combined SLA and SST data sets clearly depict different current regimes and bifurcations, which provides the basis for a new conceptual model of the seasonal circulation scheme for the Central Mediterranean. This analysis includes variations of the path and temporal behavior of the main regional circulation features (i.e., the Atlantic Tunisian Current, the Atlantic Ionian Stream, the Atlantic Libyan Current, and the Sidra Gyre), along with a new coastal current over the Gulf of Gabes (see Jebri et al. 2016 for more details).

In the Gulf of St. Lawrence, details of the circulation are also revealed by specialized processing, in this case the one adopted for the PEACHI data set. Figure 11.15 compares the cross-track velocities derived from standard processing with those from PEACHI data, with both overlain on satellite-derived surface chlorophyll concentrations. The greater detail in the PEACHI-derived velocities is consistent with advection of the surface chlorophyll field.

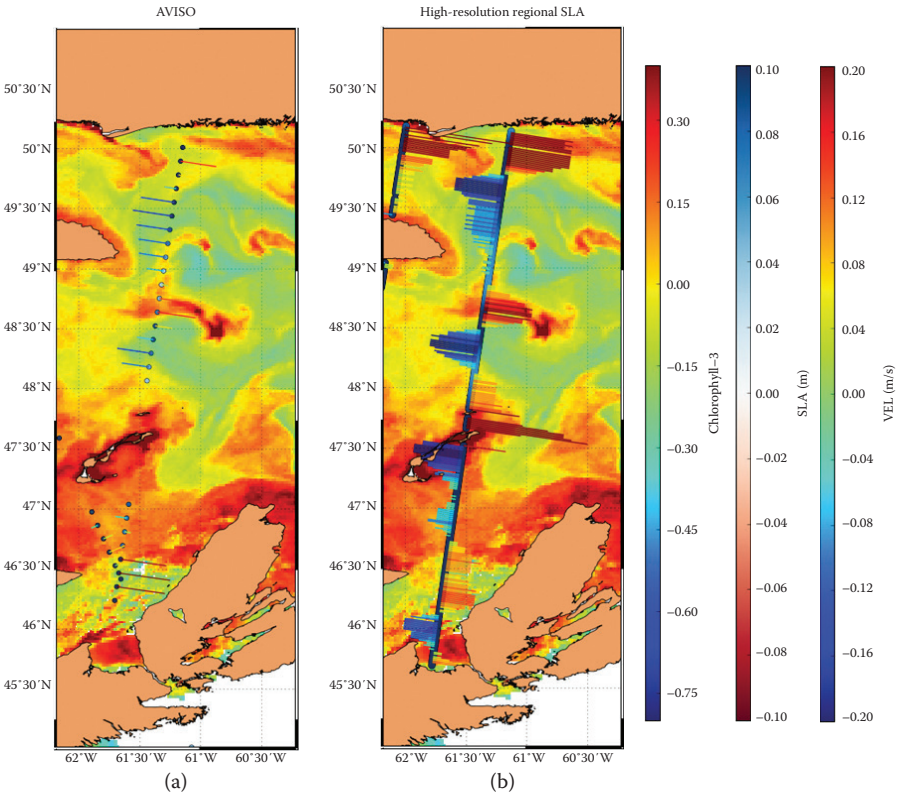

FIGURE 11.15 Ocean color image for September 8, 2014, with across-track geostrophic velocities computed from altimeter SLA. AVISO global data set (a), and high-resolution regional SLA (b). (Figure courtesy of C. Dufau, Collecte Localisation Satellite / Fisheries and Oceans Canada.)

Decreased SLA next to the coast is an indicator of wind-driven upwelling, as demonstrated along the Bonnie coast off southeast Australia (Cahill and Dufau 2015). In this study, PEACHI data allowed analysis of along-track SLA data close to the coast, which documented decreased coastal sea levels during a wind-driven upwelling event during November 2013, in agreement with colder satellite SST fields and coastal radar current fields showing surface flow to the northwest (Figure 11.16). Other studies have revealed low coastal sea levels associated with upwelling off Vietnam (Kuo et al. 2004) and in the coastal regions of the major eastern boundary currents (Strub et al. 2013).

Risien and Strub (2016) take a different approach to the improvement of sea-level fields along the U.S. West Coast. Following Saraceno et al. (2008), they blend tide gauge and altimeter data in the 75-km region next to the coast. This recaptures much of the greater energy observed with current meters over the coast, energy that is missing in geostrophic velocities calculated from standard gridded altimeter fields.

On the shortest timescales, papers by Madsen et al. (2007, 2015) have blended tide gauge and altimeter data to predict storm surge magnitudes in the complex region connecting the North Sea and Baltic Sea with multilinear regression models, anticipating more deterministic predictions using numerical circulation models. A similar statistical approach has been used to predict sea levels along the northwest coast of Britain by Cheng et al. (2012). Other very short timescale phenomena include tsunami wave elevations, which may be caught by opportunistic altimeter passes, such as reported by Troitskaya and Ermakov (2008). Another example of relatively short-term changes in sea level include the effects of expansion due to the heat content of eddies or other water masses. The influence of ocean surface heat content on the strength of tropical cyclones is now well

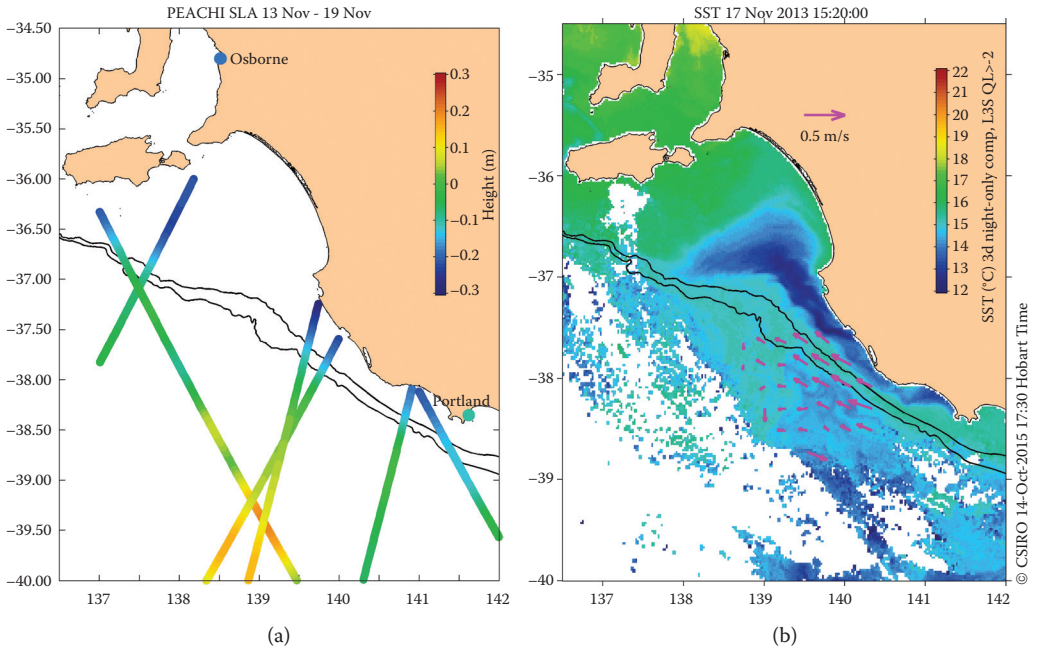

FIGURE 11.16 Along-track altimeter SLA (a) from November 13 to 19, 2013, compared to an SST image taken on November 17 (b). Altimeter data in (a) are SLA PEACHI products using Jason-2 and SARAL/AltiKa observations provided by CNES. Data in (b) are SST from the Australian Integrated Marine Observing System. Pink arrows display high-frequency (HF) radar velocities measured for the same day. Figure courtesy of M. Cahill, Commonwealth Scientific and Industrial Research Organisation (CSIRO).

documented and used in predictions of hurricane intensity (Halliwell et al. 2015) as happened in Hurricane Katrina (Scharroo et al. 2005). SLA is also useful as an indicator of ocean heat content due to El Niño signals in the California Current (Wilczak et al. 2007).

In addition to sea level and geostrophic velocities, estimates of significant wave height are derived from the slope of the leading edge of the return radar signal. These have been used in several studies to both evaluate the satellite estimates and infer properties of the coastal ocean wave field. In three tropical coastal regions, Hithin et al. (2015) found significant wave height estimates from the SARAL/AltiKa and Jason-2 altimeters compare well with *in situ* measurements. Comparing ERS-2, Envisat, Jason-1, and Jason-2 to significant wave heights at stations along the Indian coast, Jason-2 produced the best agreement with *in situ* measurements. Gridded, multi-mission data sets consistently overestimated the significant wave heights; the poorest agreement was found at the wave buoy closest to the coast. For significant wave heights less than 0.5 m, the satellite estimates were unreliable. Differences between the altimeters make it problematic to determine long-term changes in wind wave heights, as suggested by Dragani et al. (2010) along the southeast coast of South America.

For operational applications, along-track altimeter significant wave height estimates are routinely used by the U.S. NOAA NWS NCEP Ocean Prediction Center (OPC; http://www.opc.ncep.noaa.gov) for their open ocean analyzes and predictions. Data from all available altimeters (U.S. and international) are displayed by themselves and as overlays on satellite and forecast model fields (winds and waves). Near real-time data help forecasters to: determine if a specific weather system is behaving as models have predicted; observe conditions over data sparse areas; and correct large-scale biases in wave models. The altimeter data complement other data sources such as buoy winds and waves, scatterometer winds, satellite imagery and integrated displays with complimentary observations, imagery, and numerical model output. For coastal regions inshore of approximately 110 km (60 nm), the use of the wave data is more limited, due to its sparse

sampling (William Schneider and Joseph Sienkiewicz, pers. commun., August 2016). Altimeter SLA data are also used operationally by the U.S. Navy and NOAA, by assimilation into the global ocean circulation forecast models.

One of the newest applications of altimeter data in the nearshore coastal ocean is to estimate the discharge of large rivers into the ocean from the altimetry-derived river heights, which is especially promising when looking forward to the availability of swath altimeter data. Most of the investigations conducted so far are proof of concept studies, using other sources of data to approximate what is expected from the swath altimeters (Durand et al. 2014; Yoon et al. 2016). Actual estimates, however, have been made by Papa et al. (2010, 2012) for the very large discharge of the Ganga-Brahmaputra River system into the Bay of Bengal. Using T/P, ERS-2, and Envisat data for 1993 to 2008 (Papa et al. 2010) and extending the time series to 2011 using Jason-2 data (Papa et al. 2012), they find errors in the discharge estimate of 17% for 1993–2011, within the requirements of 15% to 20%. The interannual standard deviation of 12,300 $m^3\ s^{-1}$ is much larger than the data set uncertainties of 2,180 $m^3\ s^{-1}$ for the Brahmaputra and 1,458 $m^3\ s^{-1}$ for the Ganga River. Combinations of new methods for altimeter-derived estimates of river discharge and river hydrology are expected to lead to better model predictions for floods and coastal inundations (Pedinotti et al. 2014). Synergy between these and the improved predictions of storm surges described earlier will provide advance warning for the growing human populations in coastal regions.

11.6 INTEGRATION OF COASTAL ALTIMETRY IN COASTAL OBSERVING SYSTEMS

Hydrodynamic models of coastal oceanography augment observing systems by extending the spatial and temporal scope of data—notably, to sub-surface depths in the case of satellite observations and also beyond the duration of typical sustained time series platform deployments. Hydrodynamic models offer the ability to deliver long retrospective analyzes and, importantly, future predictions. When operated as real-time forecast systems, models assist decision-making for water quality, public health, maritime operations, and a host of other applications in coastal and littoral zones.

Reconciling model output and observations in applied coastal modeling entails model skill assessment and forecast verification by comparison to independent observations but also the formal merger of the two through data assimilation methods to derive estimates of the ocean state that are more accurate than models or observations alone. Data assimilation is common practice in Numerical Weather Prediction, and there has been substantial progress in the past decade in mesoscale ocean prediction spurred by Global Ocean Data Assimilation Experiment (GODAE) initiatives (Bell et al. 2015) in which the assimilation of satellite altimeter data features prominently, in the format of both along-track data and multi-mission blended, gridded products. But despite the progress detailed earlier in developing coastal-corrected along-track altimeter data products that extend valid data into shallow coastal seas and to within kilometers of the coast, the uptake of altimetry in mesoscale forecast systems has not been matched by comparable advances in coastal modeling.

This is not to say that altimetry has not been shown to usefully inform coastal circulation. Better-constrained mesoscale variability in boundary current regimes significantly enhances predictive skill in shelf seas. On the U.S. West Coast, assimilating altimeter data has a strong impact on the modeled transport of the California Current that flows along the shelf-break and also on SST variability adjacent to the coast (Moore et al. 2011). Other modeling systems such as those for the Gulf of Mexico (Barth et al. 2008) and East Australia (Oke et al. 2009) find the inclusion of satellite altimetry in deep water improves the fidelity of coastal currents.

In a comparison of seven real-time models (both local and global/basin) that span the U.S. East Coast Mid-Atlantic Bight, the model that assimilated coastal altimeter data was the most skillful (Wilkin and Hunter 2013), but that model also assimilated surface currents from coastal HF-radar systems and *in situ* data from a comprehensive coastal observatory. Other studies have considered

the merits of assimilating HF-radar surface currents (Paduan and Shulman 2004; Oke et al. 2009), but no study has yet systematically explored the relative merits, and complementarities, of radar currents and coastal altimetry in models. As we approach the era of wide-swath coastal altimetry, a study that characterizes the value of a fully global coastal satellite altimeter observation system versus a distributed network of rapid sample repeat local coastal HF-radar systems is urgently required.

One impediment to more widespread adoption of coastal altimetry in conjunction with truly coastal models (notionally, inside the 100-m isobath) is reconciling sea level variability as typically defined in mesoscale altimetry with added dynamics that are in important in coastal waters. High-frequency sea level variability due to tides, coastal-trapped waves, and storm surge are important drivers of coastal inundation risk. GODAE operational models, and the aforementioned regional shelf modeling systems (Barth et al. 2008; Moore et al. 2011), do not include tides or the influence of the inverse barometer (IB) effect on coastal sea level; they assimilate altimeter data from which those dynamics have been removed by the application of a Dynamic Atmosphere Correction (DAC) and harmonic tidal model. In a coastal ocean model that explicitly resolves these high-frequency dynamics, the DAC and tide correction remove a signal that should be retained in sea level data assimilation. To do otherwise would either misrepresent the model-data misfit cost function that underlies data-assimilative algorithms or demand a thoughtful re-specification of the so-called representation-error in data assimilation.

Defining absolute sea level above datum requires a consistent definition from global to coastal regimes. Even when the resolution of MDT is locally enhanced for regional and coastal applications (e.g., Rio et al. 2007), a clear definition of the altimetric mean sea surface reference level may be absent, yet reporting and predicting sea level anomaly with respect to a local geodetic datum consistent with coastal tide gauges is vital to making such predictions valuable to users.

One realm where it has been demonstrated that sea level forecast skill improves with the use of coastal altimetry is storm surge prediction. Madsen et al. (2015) use an ensemble optimal interpolation (EnOI) approach to assimilate a blended altimeter and coastal tide gauge analysis into a three-dimensional baroclinic hydrodynamic model of the Baltic and North seas achieving a reduction in RMS error of on average 20% across all sub-regions of the domain. Using a four-dimensional variational approach (Courtier 1997), De Biasio et al. (2016) assimilated coastal altimetry in a two-dimensional shallow water equation storm surge model for the Adriatic Sea. The skill improvement with assimilation was less pronounced than in the Baltic and North Sea model, which they attribute to the rather small extent of the Adriatic Sea and therefore relatively extended periods with no passes of a satellite. However, it should be noted that Madsen et al. (2015) did not explore the impact of altimetry in the absence of supporting tide gauge data in their blended sea level input data, so studies of the value of coastal altimetry alone remain inconclusive.

A further consideration is that multidecadal scale coastal model downscaling simulations require open boundary conditions from a global ocean model. Ideally, these would use a consistent configuration through the period of interest, yet many global-scale GODAE systems have altered their sea level datum, altimeter data assimilation scheme, and altimeter data processing version over the course of ongoing model configuration development. The GLORYS global ocean reanalysis (Ferry et al. 2012) for the altimetric era is an example of a model-based analysis that brings consistency and stability to products that coastal ocean modelers might adopt as boundary conditions for long regional down-scaling reanalyses.

Beyond data assimilation and prediction, ocean models can also make an important contribution to observing systems themselves through quantitative analysis of the resolution and impact of observational strategies. For example, Le Hénaff et al. (2009) used the Representer Matrix Spectrum method to contrast nadir altimeters with wide-swath altimetry in a model of the Bay of Biscay, finding the latter significantly superior in its ability to constrain coastal circulation physics yet also highlighting the significant influence of adding complementary *in situ* vertical profile observations of velocity and temperature.

Efforts to build upon these experiences are being promoted by several communities of practice in coastal modeling and observing. The GODAE OceanView Coastal Ocean and Shelf Seas Task Team (COSS-TT), the Coastal Altimetry Workshop (CAW) community, and their inaugural joint Altimetry for Regional and Coastal Ocean Modeling (ARCOM) workshop in 2015, have collectively voiced the desire for an agreed "best" set of coastal-corrected sea level anomaly data that removes the necessity for specialist knowledge of altimetry on the part of model users, and also gridded multi-mission sea level and/or surface current products (Kourafalou et al. 2015) that are accurate globally for the many typical coastal physical oceanography applications.

11.7 CONCLUSIONS

This chapter has described the technical advances and the applications that are making coastal altimetry a reality. It should be apparent from what has been presented that this relatively new discipline is still largely at an experimental status, and that there is room for further improvements, but this challenge is naturally presented by the peculiarities of the coastal domain. Altimetry over the open ocean has long had a mature, fully operational status, and can often be used by itself for the description of ocean dynamics at meso- and large scales and at sea level; conversely, its extension into the coastal zone, where the spatial and temporal scales decrease, naturally calls for the integration of the altimetric measurements with *in situ* observations and models, in order to mitigate for the limitations of altimetric sampling. The scope for integrating altimetry in coastal observing systems becomes strikingly clear when one considers its global coverage of the coasts and the availability of long time series that allow a robust statistical description of the variability of the coastal sea level, SWH and wind fields. Moreover, altimeters provide absolute measurements of sea level (i.e., not affected by land movement) that complement tide gauges and can in principle help derive the vertical land movement and close the link between the open observations of sea level (one of the best indicators of the changes occurring in the climate system) and those at the coast.

As the impacts of global change in the oceans are felt most severely at the coast, it is not surprising that the research community has multiplied efforts to make altimetry more usable in this crucial domain. This chapter has clearly shown that several research products are available, from a number of research groups, covering different missions and regions. The coastal altimetry community is working hard to apply these products to a number of studies, for different processes. The intense activities of calibration and validation of the various coastal altimetry data sets will hopefully lead to a convergence of the many currently available data sets into a small number of well-documented products, facilitating their uptake by the user community, including the regional and coastal modelers.

The prospects for coastal altimetry are very good—not just by virtue of all these activities but also because the evolution of altimetry as a whole is moving toward systems that have intrinsically better coastal altimetry capabilities. SAR altimetry, convincingly demonstrated by CryoSat-2, is now available over the global ocean from Sentinel-3A and allows better signal-to-noise and higher resolution that, in turn, benefit in particular the coastal observations. Another quantum leap is expected in the next decade with the arrival of full two-dimensional altimetry from SWOT. In the meantime, technical and algorithmic developments from coastal altimetry are challenging our understanding of the short scales over the open ocean, too, and may result in a better quantification of the sub-mesoscales that are of great important for biophysical interactions and ocean/atmosphere exchange.

The coastal altimetry community (http://www.coastalt.eu/community) remains very lively, and this is demonstrated by the success of the Coastal Altimetry Workshop, the tenth edition of which (CAW-10) was held in Florence, Italy, in February 2017, with more than 100 participants. This is very promising to ensure that coastal altimetry makes a real impact for coastal oceanographers, modelers, and climate scientists.

ACKNOWLEDGMENT

We thank Madeleine Cahill, Claire Dufau, Jesus Gómez-Enri, Fatma Jebri and Bruno Picard for providing some of the figures.

REFERENCES

Ablain, M., Cazenave, A., Larnicol, G., Balmaseda, M., Cipollini, P., Faugère, Y., Fernandes, M. J., Henry, O., Johannessen, J. A., Knudsen, P., Andersen, O., Legeais, J., Meyssignac, B., Picot, N., Roca, M., Rudenko, S., Scharffenberg, M. G., Stammer, D., Timms, G., & Benveniste, J. (2015). Improved sea level record over the satellite altimetry era (1993–2010) from the Climate Change Initiative project. Ocean Science, 11(1), 67–82, https://doi.org/10.5194/os-11-67-2015.

Andersen, O. (2010). The DTU10 gravity field and mean sea surface. *Second international symposium of the gravity field of the Earth (IGFS2).* Fairbanks, AK: University of Alaska, Fairbanks.

Andersen, O. B., & Scharroo, R. (2011). Range and geophysical corrections in coastal regions: And implications for mean sea surface determination. In *Coastal Altimetry* (eds. S. Vignudelli, A. Kostianoy, P. Cipollini, J. Benveniste), pp. 103–145. Berlin, Heidelberg: Springer.

Atlas, R., & Hoffman, R. N. (2000). The use of satellite surface wind data to improve weather analysis and forecasting at the NASA Data Assimilation Office. In *Satellite Oceanography and Society* (ed. D. Halpern). *Elsevier Oceanography Series*, Volume 63, pp. 57–78. Amsterdam: Elsevier Science.

Bao, L., Lu, Y., & Wang, Y. (2009). Improved retracking algorithm for oceanic altimeter waveforms. *Progress in Natural Science*, 19, 195–203. doi:10.1016/j.pnsc.2008.06.017.

Barale, V., Gower, J. F. R., & Alberotanza, L. (Eds.). (2010). *Oceanography from Space: Revisited*. Dordrecht, The Netherlands: Springer Science & Business Media.

Barth, A., Alvera-Azcárate, A., & Weisberg, R. H. (2008). Assimilation of high frequency radar currents in a nested model of the West Florida Shelf. *Journal of Geophysical Research*, 113, C08033. doi:10.1029/2007JC004585.

Bell, M. J., Schiller, A., Le Traon, P. Y., Smith, N. R., Dombrowsky, E., & Wilmer-Becker, K. 2015. An introduction to GODAE OceanView. *Journal of Operational Oceanography*, 8(suppl 1), s2–11. doi:10.1080/1755876X.2015.1022041

Bennartz, R. (1999). On the use of SSM/I measurements in coastal regions. *Journal of Atmospheric and Oceanic Technology*, 16(4), 417–431. doi:10.1175/1520-0426(1999)016<0417:OTUOSI>2.0.CO;2.

Berry, P., Freeman, J., & Smith, R. (2010). An enhanced ocean and coastal zone retracking technique for gravity field computation. In *Gravity, Geoid and Earth Observation* (ed. S. Mertikas), pp. 213–220. Berlin, Heidelberg: Springer-Verlag.

Birol, F., Cancet, M., & Estournel, C. (2010). Aspects of the seasonal variability of the Northern Current (NW Mediterranean Sea) observed by altimetry. *Journal of Marine Systems*, 81(4), 297–311. doi:10.1016/j.jmarsys.2010.01.005.

Birol F., Fuller N., Lyard F., Cancet M., Niño F., Delebecque C., Fleury S., et al. (2016). Coastal applications from nadir altimetry: Example of the X-TRACK regional products. *Advances in Space Research*, 59, 936–953. doi:10.1016/j.asr.2016.11.005.

Boehm, J., Heinkelmann, R., & Schuh, H. (2007). Short note: A global model of pressure and temperature for geodetic applications. *Journal of Geodesy*, 81, 679–683. doi:10.1007/s00190-007-0135-3.

Bouffard, J., Renault, L., Ruiz, S., Pascual, A., C. Dufau, C., & Tintore, J. (2012). Sub-surface small-scale eddy dynamics from multi-sensor observations and modeling. *Progress in Oceanography*, 106, 62–79. doi:10.1016/j.pocean.2012.06.007.

Bouffard, J., Roblou, L., Birol, F., Pascual, A., Fenoglio-Marc, L., Cancet, M., Morrow, R., & Ménard, Y. (2011). Introduction and assessment of improved coastal altimetry strategies: Case study over the Northwestern Mediterranean Sea. In *Coastal Altimetry* (eds. S. Vignudelli, A. Kostianoy, P. Cipollini, J. Benveniste), pp. 297–330. Berlin, Heidelberg: Springer.

Brown, G. (1977). The average impulse response of a rough surface and its applications. *IEEE Transactions on Antennas and Propagation*, 25, 67–74. doi:10.1109/TAP.1977.1141536.

Brown, S. (2010). A novel near-land radiometer wet path-delay retrieval algorithm: Application to the Jason-2/OSTM advanced microwave radiometer. *IEEE Transactions on Geoscience and Remote Sensing*, 48(4), 1986. doi:10.1109/TGRS.2009.2037220.

Caballero, A., Pascual, A., Dibarboure, G., & Espino, M. (2008). Sea level and Eddy Kinetic Energy variability in the Bay of Biscay, inferred from satellite altimeter data. *Journal of Marine Systems*, *72*(1), 116–134.

Cahill, M., & Dufau, C. (2015). Monitoring Coastal Upwelling using Altimetry: A Feasibility Study. 9th Coastal Altimetry Workshop, Reston (USA), 18–19 October, 2015.

Calafat, F. M., Gomis D., & Marcos, M. (2009). Comparison of Mediterranean sea level fields for the period 1961–2000 as given by a data reconstruction and a 3D model. *Global Planetary Change*, 68, 175–184. doi:10.1016/j.gloplacha.2009.04.003.

Carrère, L., & Lyard, F. (2003). Modeling the barotropic response of the global ocean to atmospheric wind and pressure forcing-comparisons with observations. *Geophysical Research Letters*, 30(6), 1275. doi:10.1029/2002GL016473.

Chang, E. T. Y., Chao, B. F., Chiang, C.-C., & Hwang, C. (2012). Vertical crustal motion of active plate convergence in Taiwan derived from tide gauge, altimetry, and GPS data. *Tectonophysics*, 578, 98–106. doi:10.1016/j.tecto.2011.10.002.

Chelton, D. B., Gaube, P., Schlax, M. G., Early, J. J., & Samelson, R. M. (2011a). The influence of non-linear mesoscale eddies on near-surface oceanic chlorophyll, *Science*, 334, 328. doi:10.1126/science.1208897.

Chelton, D. B., Schlax, M. G., & Samelson, R. M. (2011b). Global observations of non-linear mesoscale eddies. *Progress in Oceanography*, 91, 167–216. doi:10.1016/j.pocean.2011.01.002.

Cheng, Y., Andersen, O. B., & Knudsen, P. (2012). Integrating non-tidal sea level data from altimetry and tide gauges for coastal sea level prediction. *Advances in Space Research*, 50(8), 1099–1106. doi:10.1016/j.asr.2011.11.016.

Church, J. A., & White, N. J. (2006). A 20th century acceleration in global sea-level rise. *Geophysical Research Letters*, 33, L01602. doi:1029/2005GL024826.

Church, J. A., White, N. J., Coleman, R., Lambeck, K., & Mitrovica, J. X. (2004). Estimates of the regional distribution of sea level rise over the 1950–2000 period. *Journal of Climate*, 17(13), 2609–2625. doi:10.1175/1520-0442.

Cipollini, P., & Calafat, F. (2016). Altimeter processing and data for Sea Level SpaceWatch Phase 2. Sea Level SpaceWatch Workshop, 22nd March 2016, National Oceanography Centre, Southampton. Available at http://www.satoc.eu/projects/sealevelsw/docs/SLSW2_finalWS_Altimeter_results.pdf. Accessed 24 July 2017.

Cipollini, P., Calafat, F. M., Jevrejeva, S., Melet, A., & Prandi, P. (2017). Monitoring sea level in the coastal zone with satellite altimetry and tide gauges. *Surveys in Geophysics*, 38, 33. doi:10.1007/s10712-016-9392-0.

COASTALT. (2009). Wet Tropospheric Corrections in Coastal Areas, COASTALT CCN2, Deliverable D2.1b v 1.2., 30/06/2009. Document code COASTALT-D21b-12.

Courtier, P. (1997). Dual formulation of four-dimensional variational assimilation. *Quarterly Journal of the Royal Meteorological Society*, 123(544), 2449–2461. doi:10.1002/qj.49712354414.

Davis, J. L., Herring, T. A., Shapiro, I. I., Rogers, A. E. E., & Elgered, G. (1985). Geodesy by radio interferometry: effects of atmospheric modelling errors on estimates of baseline length. *Radio Science*, 20(6), 1593–1607. doi:10.1029/RS020i006p01593.

De Biasio, F., Vignudelli, S., della Valle, A., Umgiesser, G., Bajo, M., & Zecchetto, S. (2016). Exploiting the potential of satellite microwave remote sensing to hindcast the storm surge in the Gulf of Venice. *IEEE Journal of Selected Topics in Applied Earth Observations and Remote Sensing*., *9*(11), 5089–5105. doi:10.1109/JSTARS.2016.2603235.

Dee, D. P., Uppala, S. M., Simmons, A. J., Berrisford, P., Poli, P., Kobayashi, S., Andrae, U., et al. (2011). The ERA-Interim reanalysis: Configuration and performance of the data assimilation system. *Quarterly Journal of the Royal Meteorological Society*, 137, 553–597. doi:10.1002/qj.828.

Deng, X., & Featherstone, W. (2006). A coastal retracking system for satellite radar altimeter waveforms: Application to ERS-2 around Australia. *Journal of Geophysical Research*, 111(C6), C06012. doi:10.1029/2005JC003039.

Desportes, C., Obligis, E., & Eymard, L. (2007). On the wet tropospheric correction for altimetry in coastal regions. *IEEE Transactions on Geoscience and Remote Sensing*, 45(7), 2139–2149. doi:10.1109/TGRS.2006.888967.

Desportes, C., Obligis, E., & Eymard, L. (2010). One-dimensional variational retrieval of the wet tropospheric correction for altimetry in coastal regions. *IEEE Transactions on Geoscience and Remote Sensing*, 48(3), 1001–1008. doi:10.1109/TGRS.2009.2031494.

Dragani, W. C., Martin, P. B., Simionato, C. G., & Campos, M. I. (2010). Are wind wave heights increasing in south-eastern south American continental shelf between 32° S and 40° S? *Continental Shelf Research*, 30(5), 481–490. doi:10.1016/j.csr.2010.01.002.

Dufau, C., Martin-Puig, C., & Moreno, L. (2011). User requirements in the coastal ocean for satellite altimetry. In *Coastal Altimetry* (eds. S. Vignudelli, A. Kostianoy, P. Cipollini, J. Benveniste), pp. 51–60. Berlin, Heidelberg: Springer.

Durand, F., Shankar, D., Birol, F., & Shenoi, S. S. C. (2008). An algorithm to estimate coastal currents from satellite altimetry: A case study for the East India. *Coastal Current. Journal of Oceanography*, 64, 831–845. doi:10.1007/s10872-008-0069-2.

Durand, M., Neal, J., Rodríguez, E., Andreadis, K. M., Smith, L. C., & Yoon, Y. (2014). Estimating reach-averaged discharge for the River Severn from measurements of river water surface elevation and slope. *Journal of Hydrology*, 511, 92–104. doi:10.1016/j.jhydrol.2013.12.050.

Egido, A. (2014). Geo-referencing of the Delay/Doppler Level-1 stack with application to coastal altimetry. 8th Coastal Altimetry Workshop, Konstanz (Germany), 23–24 October, 2014.

Feng, G., Jin, S., & Zhang, T. (2013). Coastal sea level changes in Europe from GPS, tide gauge, satellite altimetry and GRACE, 1993–2011. *Advances in Space Research*, 51(6), 1019–1028. doi:10.1016/j.asr.2012.09.011.

Feng, H., & Vandemark, D. (2011). Altimeter data evaluation in the coastal Gulf of Maine and mid-Atlantic Bight Regions. *Marine Geodesy*, 34(3–4), 340–363.

Feng, X., Tsimplis, M. N., Marcos, M., Calafat, F. M., Zheng, J., Jordà, G., & Cipollini, P. (2015). Spatial and temporal variations of the seasonal sea level cycle in the northwest Pacific. *Journal of Geophysical Research: Oceans*, 120(10), 7091–7112. doi:10.1002/2015JC011154.

Fernandes, M. J., Bastos, L., & Antunes, M. (2003). Coastal satellite altimetry—Methods for data recovery and validation. In *Gravity and Geoid 2002,* Proceedings of 3rd Meeting of the international Gravity and Geoid commission (ed. I. N. Tziavos), pp. 302–307. Thessaloniki: Ziti.

Fernandes M. J., & Lázaro, C. (2016). GPD+ Wet Tropospheric Corrections for CryoSat-2 and GFO altimetry missions. *Remote Sensing*, 8(10), 851. doi:10.3390/rs8100851.

Fernandes, M. J., Lázaro, C., Ablain, M., & Pires, N. (2015). Improved wet path delays for all ESA and reference altimetric missions. *Remote Sensing of Environment*, 169, 50–74. doi:10.1016/j.rse.2015.07.023.

Fernandes, M. J., Lazaro, C., Nunes, A. L., Pires, N., Bastos, L., & Mendes, V. B. (2010). GNSS-derived path delay: An approach to compute the wet tropospheric correction for coastal altimetry. *IEEE Geoscience and Remote Sensing Letters*, 7(3), 596–600.

Fernandes, M. J., Lázaro, C., Nunes, A. L., & Scharroo, R. (2014). Atmospheric corrections for altimetry studies over inland water. *Remote Sensing*, 6(6), 4952–4997.

Ferry, N., Parent, L., Garric, G., Bricaud, C., Testut, C.-E., Le Galloudec, O., Lellouche, J.-M., et al. (2012). GLORYS2V1 global ocean reanalysis of the altimetric era (1992–2009) at mesoscale. *Mercator Quarterly Newsletter* 44, 29–39.

Garzoli, S. L., & Goni, G. J. (2000). Combining altimeter observations and oceanographic data for ocean circulation and climate studies. In *Satellite Oceanography and Society* (ed. D. Halpern). Elsevier Oceanography Series, Volume 63, pp. 79–97. Amsterdam: Elsevier Science.

Gaube, P., Chelton, D. B., Samelson, R. M., Schlax, M. G., & O'Neill, L. W. (2015). Satellite observations of mesoscale eddy-induced Ekman pumping. *Journal of Physical Oceanography*, 45(1), 104–132. doi:10.1175/JPO-D-14-0032.1.

Gómez-Enri, J., Cipollini, P., Passaro, M., Vignudelli, S., Tejedor, B., & Coca, J. (2016). Coastal Altimetry Products in the Strait of Gibraltar. *IEEE Transactions on Geoscience and Remote Sensing*, 54 (9), 5455–5466. doi:10.1109/TGRS.2016.2565472.

Gómez-Enri, J., Vignudelli, S., Quartly, G. D., Gommenginger, C. P., Cipollini, P., Challenor, P. G., & Benveniste, J. (2010). Modeling ENVISAT RA-2 waveforms in the coastal zone: Case study of calm water contamination. *IEEE Geoscience and Remote Sensing Letters*, 7, 474–478. doi:10.1109/LGRS.2009.2039193.

Gommenginger, C., Thibaut, P., Fenoglio-Marc, L., Quartly, G., Deng, X., Gómez-Enri, J., Challenor, P., & Gao, Y. (2011). Retracking altimeter waveforms near the coasts. In *Coastal Altimetry* (eds. Vignudelli et al.), pp. 61–101. Berlin, Heidelberg: Springer.

Guo, J., Gao, Y., Hwang, C., & Sun, J. (2010). A multi-subwaveform parametric retracker of the radar satellite altimetric waveform and recovery of gravity anomalies over coastal oceans. *Science China Earth Sciences*, 610–616. doi:10.1007/s11430-009-0171-3.

Halimi, A., Mailhes, C., Tourneret, J. -Y., Thibaut, P., & Boy, F. (2013). Parameter estimation for peaky altimetric waveforms. *IEEE Transactions on Geoscience and Remote Sensing*, 1568–1577. doi:10.1109/TGRS.2012.2205697.

Halliwell, Jr., G. R., Gopalakrishnan, S., Marks, F., & Willey, D. (2015). Idealized study of ocean impacts on tropical cyclone intensity forecasts. *Monthly Weather Review*, 143(4), 1142–1165. doi:10.1175/MWR-D-14-00022.1.

Hamlington, B. D., Leben, R. R., Nerem, R. S., Han, W., & Kim, K. Y. (2011). Reconstructing sea level using cyclostationary empirical orthogonal functions. *Journal of Geophysical Research: Oceans*, 116(C12). doi:10.1029/2011JC007529.

Han, W., Meehl, G. A., Rajagopalan, B., Fasullo, J. T., Hu, A., Lin, J., Large, W. G., et al. (2010). Patterns of Indian Ocean sea-level change in a warming climate. *Nature Geoscience*, 3(8), 546–550. doi:10.1038/ngeo901.

Harwood, P. (2015). *DUE eSurge Final Report*. Ref: D430. Available at http://due.esrin.esa.int/files/20150310050027.pdf. Accessed 24 July 2017.

He, L., Li, G., Li, K., & Shu, Y. (2014). Estimation of regional sea level change in the Pearl River Delta from tide gauge and satellite altimetry data. *Estuarine, Coastal and Shelf Science*, 141, 69–77. doi:10.1016/j.ecss.2014.02.005.

Herbert, G., Ayoub, N., Marsaleix, P., & Lyard, F. (2011). Signature of the coastal circulation variability in altimetric data in the southern Bay of Biscay during winter and fall 2004. *Journal of Marine Systems*, 88(2), 139–158. doi:10.1016/j.jmarsys.2011.03.004.

Hithin, N. K., Remya, P. G., Nair, T. B., Harikumar, R., Kumar, R., & Nayak, S. (2015). Validation and intercomparison of SARAL/AltiKa and PISTACH-derived coastal wave heights using in-situ measurements. *IEEE Journal of Selected Topics in Applied Earth Observations and Remote Sensing*, 8(8), 4120–4129. doi:10.1109/JSTARS.2015.2418251.

Hopfield, H. S. (1969). Two-quartic tropospheric refractivity profile for correcting satellite data. *Journal of Geophysical Research*, 74(18), 4487–4499. doi:10.1029/JC074i018p04487.

Hwang, C., Guo, J., Deng, X., Hsu, H. -Y., & Liu, Y. (2006). Coastal gravity anomalies from retracked GEOSAT/GM altimetry: Improvement, limitation and the role of airborne gravity data. *Journal of Geodesy*, 80(4), 204–216. doi:10.1007/s00190-006-0052-x.

Idris, N., & Deng, X. (2012). The retracking technique on multi-peak and quasi-specular waveforms for Jason-1 and Jason-2 missions near the coast. *Marine Geodesy*, 217–237. doi:10.1080/01490419.2012.718679.

Ikeda, M., & Dobson, F.W. (1995). *Oceanographic Applications of Remote Sensing.* New York: CRC Press.

Janssen, P. (2000). ECMWF wave modeling and satellite altimeter wave data. In *Satellite Oceanography and Society* (ed. D. Halpern). Elsevier Oceanography Series, Volume 63, pp. 35–56. Amsterdam: Elsevier Science.

Jebri, F., Birol, F., Zakardjian, B., Bouffard, J., & Sammari, C. (2016). Exploiting coastal altimetry to improve the surface circulation scheme over the central Mediterranean Sea. *Journal of Geophysical Research: Oceans*, 121(7), 4888–4909. doi:10.1002/2016JC011961.

Karbou, F., Prigent, C., Eymard, L., & Pardo, J.R. (2005). Microwave land emissivity calculations using AMSU measurements. *IEEE Transactions on Geoscience and Remote Sensing*, 43(5), 948–959. doi:10.1109/TGRS.2004.837503.

Klemas, V. (2012). Remote Sensing of Coastal and Ocean Currents: An Overview. *Journal of Coastal Research*, 28(3), 576–586. https://doi.org/10.2112/JCOASTRES-D-11-00197.1

Kourafalou, V., De Mey, P., & Wilmer-Becker, K. (2015). Report of the 4th GODAE OceanView Coastal Ocean and Shelf Seas Task Team (COSS-TT) International Coordination Workshop (COSS-ICW4), Lisbon, Portugal, Sept. 2015. Available at https://www.godae-oceanview.org/files/download.php?m=documents&f=160204121952-ICWS4Lisbonreportfinal.pdf. Accessed 24 July 2017.

Krug, M., & Tournadre, J. (2012). Satellite observations of an annual cycle in the Agulhas Current. *Geophysical Research Letters*, 39(15), L15607. doi:10.1029/2012GL052335.

Krug, M., Tournadre, J., & Dufois, F. (2014). Interactions between the Agulhas Current and the eastern margin of the Agulhas Bank. *Continental Shelf Research*, 81, 67–79. doi:10.1016/j.csr.2014.02.020.

Kuo, N. J., Zheng, Q., & Ho, C. R. (2004). Response of Vietnam coastal upwelling to the 1997–1998 ENSO event observed by multisensor data. *Remote Sensing of Environment*, 89(1), 106–115. doi:10.1016/j.rse.2003.10.009.

Le Bars, Y., Lyard, F., Jeandel, C., & Dardengo, L. (2010). The AMANDES tidal model for the Amazon estuary and shelf. *Ocean Modelling*, 31(3), 132–149. doi:10.1016/j.ocemod.2009.11.001.

Lee, H., Shum, C. K., Emery, W., Calmant, S., Deng, X., Kuo, C.-Y., Roesler, C., & Yi, Y. (2010). Validation of Jason–2 altimeter data by waveform retracking over California coastal ocean. *Marine Geodesy*, 33, 304–316. doi:10.1080/01490419.2010.488982.

Legeais, J. F., Ablain, M., & Thao, S. (2014). Evaluation of wet troposphere path delays from atmospheric reanalyzes and radiometers and their impact on the altimeter sea level. *Ocean Science*, 10(6), 893–905. doi:10.5194/os-10-893-2014.

Le Hénaff, M., De Mey, P., & Marsaleix, P. (2009). Assessment of observational networks with the Representer Matrix Spectra method—Application to a 3D coastal model of the Bay of Biscay. *Ocean Dynamics.* 59(1), 3–20. doi:10.1007/s10236-008-0144-7.

Le Provost, C., Genco, M. L., Lyard, F., Vincent, P., & Canceil, P. (1994). Spectroscopy of the world ocean tides from a finite element hydrodynamic model. *Journal of Geophysical Research: Oceans*, 99(C12), 24777–24797. doi:10.1029/94JC01381.

Liu, Y., Weisberg, R. H., Vignudelli, S., & Mitchum, G. T. (2014). Evaluation of altimetry-derived surface current products using Lagrangian drifter trajectories in the eastern Gulf of Mexico. *Journal of Geophysical Research: Oceans*, 119(5), 2827–2842. doi:10.1002/2013JC009710.

Liu, Y., Weisberg, R. H., Vignudelli, S., Roblou, L., & Merz, C. R. (2012). Comparison of the X-TRACK altimetry estimated currents with moored ADCP and HF radar observations on the West Florida Shelf. *Advances in Space Research*, 50(8), 1085–1098. doi:10.1016/j.asr.2011.09.012.

Luu, Q. H., Tkalich, P., & Tay, T. W. (2015). Sea level trend and variability around Peninsular Malaysia. *Ocean Science*, 11(4), 617–628. doi:10.5194/osd-11-1519-2014.

Madsen, K. S., Høyer, J. L., Fu, W., & Donlon, C. (2015). Blending of satellite and tide gauge sea level observations and its assimilation in a storm surge model of the North Sea and Baltic Sea. *Journal of Geophysical Research: Oceans*, 120(9), 6405–6418. doi:10.1002/2015JC011070.

Madsen, K. S., Høyer, J. L., & Tscherning, C. C. (2007). Near-coastal satellite altimetry: Sea surface height variability in the North Sea–Baltic Sea area. *Geophysical Research Letters*, 34(14), L14601. doi:10.1029/2007GL029965.

Maraldi, C., Galton-Fenzi, B., Lyard, F., Testut, L., & Coleman, R. (2007). Barotropic tides of the southern Indian Ocean and the Amery Ice Shelf cavity. *Geophysical Research Letters*, 34(18), L18602. doi:10.1029/2007GL030900.

Marcos, M., Wöppelmann, G., Bosch, W., & Savcenko, R. (2007). Decadal sea level trends in the Bay of Biscay from tide gauges, GPS and TOPEX. *Journal of Marine Systems*, 68(3), 529–536. doi:10.1016/j.jmarsys.2007.02.006.

Melet, A., Gourdeau, L., & Verron, J. (2010). Variability in Solomon Sea circulation derived from altimeter sea level data. *Ocean Dynamics*, 60(4), 883–900. doi:10.1007/s10236-010-0302-6.

Mercier, F., Picot, N., Thibaut, P., Cazenave, A., Seyler, F., Kosuth, P., & Bronner, E. (2009). CNES/PISTACH project: An innovative approach to get better measurements over in-land water bodies from satellite altimetry. Early results. *EGU General Assembly Conference Abstracts*, 11, 11674.

Mercier, F., Picot, N., Guinle, T., Cazenave, A., Kosuth, P., & Seyler, F. (2012). The PISTACH project for coastal and hydrology altimetry: 2012 project status and activities. Presentation at 20 Years of Progress in Radar Altimetry Symposium, Venice, Italy.

Mercier, F., Rosmorduc, V., Carrere, L., & Thibaut, P. (2010). *Coastal and Hydrology Altimetry Product (PISTACH) Handbook*. CLS-DOS-NT-10-246, Issue 1.0. Toulouse: CNES.

Meyssignac, B., Becker, M., Llovel, W., & Cazenave, A. (2012). An assessment of two-dimensional past sea level reconstructions over 1950–2009 based on tide-gauge data and different input sea level grids. *Surveys in Geophysics*, 33(5), 945–972.

Miller, M., Buizza, R., Haseler, J., Hortal, M., Janssen, P., & Untch, A. (2010). Increased resolution in the ECMWF deterministic and ensemble prediction systems. *ECMWF Newsletter*, 124, 10–16.

Mitchum, G., and B. Kilonsky. (1995) Observations of tropical sea level variability from altimeters. In *Oceanographic Applications of Remote Sensing* (eds. M. Ikeda, F. W. Dobson), pp. 113–127. New York: CRC Press.

Moore, A. M., Arango, H. G., Broquet, G., Edward, C., Veneziani, M., Powell, B., Foley, D., Doyle, J., Costa, D., & Robinson, P. (2011). The Regional Ocean Modeling System (ROMS) 4-dimensional variational data assimilation systems. Part III: Observation impact and observation sensitivity in the California Current System. *Progress in Oceanography*, 91, 74–94. doi:10.1016/j.pocean.2011.05.005.

Nerem, R. S., Chambers, D. P., Hamlington, B. D., Leben, R. R., Mitchum, G. T., Phillips, T., & Willis, J. K. (2010). Observations of recent sea level change. Paper presented at the IPCC Workshop on Sea Level Rise and Ice Sheet Instabilities. Intergovernmental Panel on Climate Change, Malaysia. June 2010.

Obligis, E., Desportes, C., Eymard, L., Fernandes, M. J., Lázaro, C., & Nunes, A. L. (2011). Tropospheric corrections for coastal altimetry. In *Coastal altimetry* (eds. S. Vignudelli, A. Kostianoy, P. Cipollini, J. Benveniste), 147–176, Springer Berlin Heidelberg, doi:10.1007/978-3-642-12796-0_6.

Obligis, E., Eymard, L., Tran, N., Labroue, S., & Femenias, P. (2006). First three years of the microwave radiometer aboard Envisat: In-flight calibration, processing, and validation of the geophysical products. *Journal of Atmospheric and Oceanic Technology*, 23(6), 802–814. doi:10.1175/JTECH1878.1.

Oke, P. R., Sakov, P., & Schulz, E. (2009). A comparison of shelf observation platforms for assimilation in an eddy-resolving ocean model. *Dynamics of Atmospheres and Oceans*, 48(1), 121–142. doi:10.1016/j.dynatmoce.2009.04.002.

Oliveira, P. B., Serra, N., Fiúza, A., & Ambar, I. (2000). A Study of Mediterranean salt lenses using in situ and satellite observations. In *Satellite Oceanography and Society* (ed. D. Halpern), Elsevier Oceanography Series, Volume 63, pp. 125–148. Amsterdam: Elsevier Science.

Paduan, J. D., & Shulman, I. (2004). HF radar data assimilation in the Monterey Bay area. *Journal of Geophysical Research: Oceans*, 109(C7), C07S09. doi:10.1029/2003JC001949.

Pairaud, I. L., Lyard, F., Auclair, F., Letellier, T., & Marsaleix, P. (2008). Dynamics of the semi-diurnal and quarter-diurnal internal tides in the Bay of Biscay. Part 1: Barotropic tides. *Continental Shelf Research*, 28(10), 1294–1315. doi:10.1016/j.csr.2008.03.004.

Papa, F., Bala, S. K., Pandey, R. K., Durand, F., Gopalakrishna, V. V., Rahman, A., & Rossow, W. B. (2012). Ganga–Brahmaputra river discharge from Jason–2 radar altimetry: An update to the long–term satellite–derived estimates of continental freshwater forcing flux into the Bay of Bengal. *Journal of Geophysical Research: Oceans*, 117(C11). doi:10.1029/2012JC008158.

Papa, F., Durand, F., Rossow, W. B., Rahman, A., & Bala, S. K. (2010). Satellite altimeter-derived monthly discharge of the Ganga-Brahmaputra River and its seasonal to interannual variations from 1993 to 2008. *Journal of Geophysical Research: Oceans*, 115(C12). doi:10.1029/2009JC006075.

Passaro, M., Cipollini, P., Vignudelli, S., Quartly, G. D., & Snaith, H. M. (2014). ALES: A multi-mission adaptive subwaveform retracker for coastal and open ocean altimetry. *Remote Sensing of Environment*, 145, 173–189. doi:10.1016/j.rse.2014.02.008.

Passaro, M., Cipollini, P., & Benveniste, J. (2015a). Annual sea level variability of the coastal ocean: The Baltic Sea-North Sea transition zone. *Journal of Geophysical Research: Oceans*, 120(4), 3061–3078. doi:10.1002/2014JC010510.

Passaro, M., Dinardo, S., Quartly, G. D., Snaith, H. M., Benveniste, J., Cipollini, P., & Lucas, B. (2016). Cross-calibrating ALES Envisat and CryoSat-2 Delay–Doppler: A coastal altimetry study in the Indonesian Seas. *Advances in Space Research*, 58(3), 289–303. doi:10.1016/j.asr.2016.04.011.

Passaro, M., Fenoglio-Marc, L., & Cipollini, P. (2015b). Validation of significant wave height from improved satellite altimetry in the German Bight. *IEEE Transactions on Geoscience and Remote Sensing*, 53(4), 2146–2156.

Pedinotti, V., Boone, A., Ricci, S., Biancamaria, S., & Mognard, N. (2014). Assimilation of satellite data to optimize large-scale hydrological model parameters: A case study for the SWOT mission. *Hydrology and Earth System Sciences*, 18(11), 4485–4507. doi:10.5194/hess-18-4485-2014.

Pegliasco, C., Chaigneau, A., & Morrow, R. (2015). Main eddy vertical structures observed in the four major Eastern Boundary Upwelling Systems. *Journal of Geophysical Research: Oceans*, 120(9), 6008–6033. doi:10.1002/2015JC010950.

Picard, B., Frery, M. L., Obligis, E., Eymard, L., Steunou, N., & Picot, N. (2015). SARAL/AltiKa wet tropospheric correction: In-flight calibration, retrieval strategies and performances. *Marine Geodesy*, 38(suppl 1), 277–296. doi:10.1080/01490419.2015.1040903.

Quartly, G. D. (2010). Hyperbolic retracker: Removing bright target artifacts from altimetric waveform data. ESA SP-686, Living Planet Symposium 2010, Bergen, Norway, (28 June – 2 July, 2007). ESA Publication, SP-686. Noordwijkerhout, NL: ESA.

Reynolds, R. W, Behringer, D., Ji, M., Leetmaa, A., Maes, C., Vossepoel, F., & Xue Y. (2000). Analyzing the 1993–1998 interannual variability of NCEP model ocean simulations: The contribution of TOPEX/Poseidon observations. In *Satellite Oceanography and Society* (ed. D. Halpern). Elsevier Oceanography Series, Volume 63, pp. 299–308. Amsterdam: Elsevier Science.

Rio, M. H., Mulet, S., & Picot, N. (2014a). Beyond GOCE for the ocean circulation estimate: Synergetic use of altimetry, gravimetry, and in situ data provides new insight into geostrophic and Ekman currents. *Geophysical Research Letters*, 41(24), 8918–8925. doi:10.1002/2014GL061773.

Rio, M. H., Pascual, A., Poulain, P. M., Menna, M., Barceló-Llull, B., & Tintoré, J. (2014b). Computation of a new mean dynamic topography for the Mediterranean Sea from model outputs, altimeter measurements and oceanographic in-situ data. *Ocean Science*, 10, 731–744. doi:10.5194/os-10-731-201ence.

Rio, M.-H., Poulain, P. M., & Pascual, A., Mauri, E., Larnicol, G., & Santoleri, R. (2007). A mean dynamic topography of the Mediterranean Sea computed from altimetric data, in-situ measurements and a general circulation model. *Journal of Marine Systems*, 65, 484–508. doi:10.1016/j.jmarsys.2005.02.006.

Risien, C. M., & Strub, P. T. (2016). Blended sea level anomaly fields with enhanced coastal coverage along the US West Coast. *Scientific Data*, 3, 160013. doi:10.1038/sdata.2016.13.

Roblou, L., Lamouroux, J., Bouffard, J., Lyard, F., Le Hénaff, M., Lombard, A., Marsaleix, P., De Mey P., & Birol, F. (2011). Post-processing altimeter data towards coastal applications and integration into coastal models. In *Coastal Altimetry* (eds. S. Vignudelli, A. Kostianoy, P. Cipollini, J. Benveniste), pp. 217–246. Berlin, Heidelberg: Springer.

Ruf, C. S., & Giampaolo, J. C. (1998). Littoral antenna deconvolution for a microwave radiometer. *Proceedings of 1998 International Geoscience and Remote Sensing Symposium*, Seattle, WA, Cat. #98CH36174, 378–380. Doi:10.1109/IGARSS.1998.702911.

Ruiz Etcheverry, L. A., Saraceno, M., Piola, A. R., & Strub, P. T. (2016). Sea level anomaly on the Patagonian continental shelf: Trends, annual patterns and geostrophic flows. *Journal of Geophysical Research: Oceans*, 121(4), 2733–2754. doi:10.1002/2015JC011265.

Saraceno, M., Strub, P. T., & Kosro, P. M. (2008). Estimates of sea surface height and near-surface alongshore coastal currents from combinations of altimeters and tide gauges. *Journal of Geophysical Research: Oceans*, 113(C11). doi:10.1029/2008JC004756.

Scharroo, R., Lillibridge, J. L., Smith, W. H. F., & Schrama, E. J. O. (2004). Cross-calibration and long-term monitoring of the microwave radiometers of ERS, TOPEX, GFO, Jason, and Envisat. *Marine Geodesy*, 27(1–2), 279–297. doi:10.1080/01490410490465265.

Scharroo, R., Smith, W. H., & Lillibridge, J. L. (2005). Satellite altimetry and the intensification of Hurricane Katrina. *Eos, Transactions American Geophysical Union*, 86(40), 366–366. doi:10.1029/2005EO400004.

Stammer, D., Cazenave, A., Ponte, R. M., & Tamisiea, M. E. (2013). Causes for contemporary regional sea level changes. *Annual Review of Marine Science*, 5, 21–46.

Stammer, D., Ray, R. D., Andersen, O. B., Arbic, B. K., Bosch, W., Carrere, L., Cheng, Y., et al. (2014). Accuracy assessment of global barotropic ocean tide models. *Reviews of Geophysics*, 52, 243–282. doi:10.1002/2014RG000450.

Steunou, N., Desjonquères, J. D., Picot, N., Sengenes, P., Noubel, J., & Poisson, J. C. (2015). AltiKa altimeter: Instrument description and in flight performance. *Marine Geodesy*, 38(suppl 1), 22–42. doi:10.1080/01490419.2014.988835.

Strub, P. T., Combes, V., Shillington, F. A., & Pizarro, O. (2013). Currents and processes along the eastern boundaries. In *Ocean Circulation and Climate: A 21st Century Perspective* (eds. G. Siedler, S. M. Griffies, J. Gould, J. A. Church), pp. 339–384. Oxford: Academic Press.

Strub, P. T., James, C., Combes, V., Matano, R. P., Piola, A. R., Palma, E. D., Saraceno, M., Guerrero, R., Fenco, H., & Ruiz-Etcheverry, L. A. (2015). Altimeter-derived seasonal circulation on the southwest Atlantic shelf: 27°–43° S. *Journal of Geophysical Research: Oceans*, 120(5), 3391–3418. doi:10.1002/2015JC010769.

Thibaut, P., Aublanc, J., Moreau, T., Boy, F., & Picot, N. (2014). Delay/Doppler Waveform Processing in Coastal Zones. 8th Coastal Altimetry Workshop, Konstanz (Germany), 23–24 October, 2014.

Tournadre, J., Chapron, B., Reul, N., & Vandemark, D. C. (2006). A satellite altimeter model for ocean slick detection. *Journal of Geophysical Research*, 111, C04004. doi:10.1029/2005JC003109.

Tournadre, J., Whitmer, K., & Girard-Ardhuin, F. (2008). Iceberg detection in open water by altimeter waveform analysis. *Journal of Geophysical Research*, 113, C08040. doi:10.1029/2007JC004587.

Troitskaya, Y. I., & Ermakov, S. A. (2008). Manifestations of the Indian Ocean tsunami of 2004 in satellite nadir–viewing radar backscatter variations. *Geophysical Research Letters*, 33(4). L04607. doi:10.1029/2005GL024445.

Valladeau, G., Thibaut, P., Picard, B., Poisson, J. C., Tran, N., Picot, N., & Guillot, A. (2015). Using SARAL/AltiKa to improve Ka-band altimeter measurements for coastal zones, hydrology and ice: The PEACHI prototype. *Marine Geodesy*, 38(suppl 1), 124–142. doi:10.1080/01490419.2015.1020176.

Valladeau, G., Thibaut, P., Picot, N., Guillot, A., Boy, F., Le Gac, S., & the PEACHI team. (2016). *PEACHI Project: Improving Ka-Band Altimeter Measurements*. Prague: ESA Living Planet.

Vignudelli, S., Cipollini, P., Roblou, L., Lyard, F., Gasparini, G. P., Manzella, G., & Astraldi, M. (2005). Improved satellite altimetry in coastal systems: Case study of the Corsica Channel (Mediterranean Sea). *Geophysical Research Letters*, 32(7). L07608. doi:10.1029/2005GL022602.

Vignudelli, S., Kostianoy, A. G., Cipollini, P., & Benveniste J. (Eds). (2011). *Coastal Altimetry*. Berlin Heidelberg: Springer-Verlag, 578 p., doi:10.1007/978-3-642-12796-0.

Wentz, F. J. (2013). *SSM/I Version-7 Calibration Report*. Remote Sensing Systems Technical Report, 11012, 46. Santa Rosa, Calif.: Remote Sensing Systems.

Wijesekera, H. W., Jensen, T. G., Jarosz, E., Teague, W. J., Metzger, E. J., Wang, D. W., Jinadasa, S. U. P., Arulananthan, K., Centurioni, L. R., & Fernando, H. J. S. (2015). Southern Bay of Bengal currents and salinity intrusions during the northeast monsoon. *Journal of Geophysical Research: Oceans*, 120(10), 6897–6913. doi:10.1002/2015JC010744.

Wilczak, J. M., Leben, R. R., & McCollum, D. S. (2007). Upper-ocean thermal structure and heat content off the US West Coast during the 1997–1998 El Niño event based on AXBT and satellite altimetry data. *Progress in Oceanography*, 74(1), 48–70. doi:10.1016/j.pocean.2007.02.006.

Wilkin, J., & Hunter, E. (2013). An assessment of the skill of real-time models of middle Atlantic Bight continental shelf circulation. *Journal of Geophysical Research*, 118, 2919–2933. doi:10.1002/jgrc.20223223.

Wöppelmann, G., & Marcos, M. (2016). Vertical land motion as a key to understanding sea level change and variability. *Reviews of Geophysics*, 54(1), 64–92.

Yang, L., Lin, M., Liu, Q., & Pan, D. (2012). A coastal altimetry retracking strategy based on waveform classification and subwaveform extraction. *International Journal of Remote Sensing*, 33, 7806–7819.

Yang, Y., Hwang, C., Hsu, H., Dongchen, E., & Wang, H. (2011). A subwaveform threshold retracker for ERS-1 altimetry: A case study in the Antarctic Ocean. *Computers and Geosciences*, 41, 88–98.

Yildiz, H., Andersen, O. B., Simav, M., Aktug, B., & Ozdemir, S. (2013). Estimates of vertical land motion along the southwestern coasts of Turkey from coastal altimetry and tide gauge data. *Advances in Space Research*, 51(8), 1572–1580. doi:10.1016/j.asr.2012.11.011.

Yoon, Y., Garambois, P. A., Paiva, R. C., Durand, M., Roux, H., & Beighley, E. (2016). Improved error estimates of a discharge algorithm for remotely sensed river measurements: Test cases on Sacramento and Garonne Rivers. *Water Resources Research*, 52(1), 278–294. doi:10.1002/2015WR017319.